A novel knock sideways approach for *Plasmodium* secreted proteins reveals a surprising insensitivity to vacuolar depletion of PTEX component HSP101

Manuel A Fierro[1], Tahir Hussain[1], Liam J Campin[2] and Josh R Beck[1,2*]

[1]Department of Biomedical Sciences, Iowa State University, Ames, IA, 50011, USA

[2]Roy J. Carver Department of Biochemistry, Biophysics and Molecular Biology, Iowa State University, Ames, IA, 50011, USA

[*]Corresponding author: jrbeck@iastate.edu

Abstract

Obligate intracellular malaria parasites depend on protein secretion to penetrate, subvert, and exit their host cells. Despite this key reliance on the secretory pathway, none of the conditional mutagenesis tools available in *Plasmodium spp.* exploit the unique trafficking features of secreted proteins. Here we report knockER, a novel DiCre-mediated knock sideways approach that sequesters secreted proteins in the ER via conditional fusion of a KDEL ER-retrieval sequence to the target protein C-terminus. We applied knockER to a diverse set of reporters and endogenous *P. falciparum* and *P. berghei* proteins targeted to the rhoptries, dense granules, parasite vacuole and apicoplast and show conditional ER sequestration is not generally toxic, enabling loss-of-function studies. Taking advantage of the unique ability to redistribute secreted protein pools from their terminal destination to the ER, we employed knockER to study components of the PTEX translocon in an attempt to separate HSP101 vacuolar function in protein export from a recently proposed role in cargo recognition at the ER. Strikingly, while KDEL-fusion produced similar levels of ER retrieval for both HSP101 and the translocon adaptor PTEX150, parasite growth and effector export were completely unaffected by HSP101 retention while ER retrieval of PTEX150 produced a lethal export defect, indicating vacuolar HSP101 levels are uniquely maintained in excess. Intriguingly, redistribution of HSP101 to the ER did not further sensitize parasites to TetR-DOZI-mediated knockdown compared to parasites containing normal vacuolar levels of HSP101, suggesting PV-localized function does not fully account for HSP101 contribution to parasite fitness and consistent with an important role for HSP101 in the ER. Collectively, our work provides a novel tool for dissecting secreted protein function with sub-compartmental resolution that should be widely amenable to genetically tractable eukaryotes.

41 **Introduction**

42 Protein secretion is a fundamental biological process of all living cells. In eukaryotes this
43 is accomplished by a dedicated secretory pathway that begins with import into the Endoplasmic
44 Reticulum (ER) for initial folding and post-translational modification, followed by sorting in the
45 Golgi and post-Golgi compartments. As an obligate intracellular parasite, secreted proteins play
46 a critical role in the biology of the malaria parasite, *Plasmodium*. Through the secretory pathway,
47 proteins are trafficked into both the plasma membrane and several organelles, including a relict
48 plastid called the apicoplast that is critical for parasite metabolism (1). During schizogony, another
49 subset of proteins is packaged into several distinct secretory organelles that are subsequently
50 discharged to facilitate host cell attachment and penetration (2). Invagination of the host
51 membrane by the parasites during invasion generates an intracellular microenvironment called
52 the parasitophorous vacuole (PV) which forms the interface for host-parasite interactions (3).
53 Resident PV proteins secreted into the vacuole perform critical functions at this interface,
54 including nutrient/waste exchange and protein export (4). The later process enables parasites to
55 deploy a battery of secreted effector proteins across the PV membrane (PVM) and into the host
56 compartment, dramatically remodeling the erythrocyte to meet nutritional demands and avoid host
57 defenses (5, 6). Remarkably, it is estimated that up to 10% of the parasite genome is devoted to
58 encoding exported effectors, further highlighting the central importance of protein secretion to this
59 parasitic lifestyle (7-11).

60 Despite their divergent position as early branching eukaryotes, *Plasmodium spp.* and
61 other apicomplexan parasites have retained many of the canonical features of the secretory
62 pathway (12). Like other eukaryotes, entry into the secretory pathway generally begins with co-
63 translational import of proteins containing a signal peptide or transmembrane domain(s) into the
64 ER via the Sec61 complex, followed by sorting from the Golgi to internal compartments, the PV
65 or beyond into the host (13). ER-resident proteins that escape the ER via bulk flow in COPII
66 vesicles are returned to the ER in COPI vesicles by ERD2 surveillance, which binds a C-terminal

67 retrieval sequence ("KDEL" and variants) in the *cis* Golgi and releases it in the ER in a pH-
68 dependent manner (14-16). Similar to other eukaryotes, ER retention of secreted reporters or
69 chimeric proteins can be achieved in *Plasmodium spp.* by a C-terminal KDEL or functional
70 variants (17-22).

71 In this present work, we developed and characterized a novel DiCre-based knock
72 sideways tool called knockER that enables conditional fusion of KDEL to the C-terminus of
73 secreted proteins, subjecting the target protein to ERD2 surveillance in the *cis* Golgi to cause its
74 retrieval to the ER. Using this approach, we show successful conditional retrieval of five
75 endogenous *Plasmodium* proteins (ClpB1, RON6, EXP2, PTEX150 and HSP101) that traffic
76 through the ER to diverse compartments including the apicoplast, rhoptries, dense granules, and
77 the PV. Importantly, conditional ER retrieval of both highly expressed reporters and endogenously
78 tagged proteins does not generally impact fitness, indicating knockER-mediated phenotypes are
79 not the indirect result of an integrated stress response, thus making this system suitable for protein
80 loss-of-function studies. Indeed, we show that knockER reproduces known loss-of-function
81 phenotypes previously established by other conditional knockdown strategies. We further apply it
82 to study loss of ClpB1 and RON6 function for the first time, revealing an essential apicoplast
83 function for the former and suggesting that RON6 is dispensable during the blood stage. Lastly,
84 we took advantage of the ability to redistribute secreted protein pools to interrogate a recently
85 proposed ER function for the PTEX translocon component HSP101 in addition to its role in the
86 PV (23). We reveal a surprising insensitivity to ER retrieval of HSP101 in contrast to the other
87 PTEX components, indicating HSP101 is maintained in excess in the PV. Interestingly, depletion
88 of HSP101 PV levels does not hypersensitize parasites to HSP101 knockdown, providing support
89 for an HSP101 function in the early secretory pathway in addition to its role in protein translocation
90 across the PVM in the assembled PTEX complex (24-26). These results establish knockER as a
91 novel tool to study secreted proteins and provide the first functional genetic evidence for an extra-

92 vacuolar HSP101 function, highlighting the unique ability of knockER to resolve function between
93 compartments for dually localized proteins.
94
95 **Results**
96 **Conditional ER retrieval of a secreted reporter does not impact parasite fitness**
97 To facilitate conditional ER retrieval of a protein of interest, we designed a strategy based
98 on the DiCre system where a gene of interest is C-terminally fused to a 3xFLAG tag and a stop
99 codon flanked by *loxP* sequences imbedded in small introns (27) which, upon addition of
100 rapamycin, undergo recombination via activation of the dimerizable Cre recombinase (27, 28).
101 Excision of the loxP-intervening sequence removes the 3xFLAG tag and stop codon and brings
102 into frame a 3xHA tag followed by the ER-retention sequence KDEL and a stop codon (Figure
103 1A). While the ER plays a crucial role in quality control and is sensitive to added stress (29, 30),
104 several previous studies have exogenously expressed various KDEL or SDEL fusion proteins in
105 *P. falciparum* and *P. berghei* without apparent impact on parasite fitness (21, 31-37). To directly
106 ascertain whether ER retrieval of a highly expressed secreted protein impacted parasite fitness,
107 we first appended the knockER system to an mNeonGreen (mNG) reporter and fused this to the
108 *exp2* 5' UTR and signal peptide, enabling expression from the strong *exp2* promoter and entry
109 into the ER followed by default secretion into the PV (38-40). This assembly was placed under
110 control of the anhydrotetracycline (aTc)-responsive TetR-DOZI-aptamers system to prevent
111 expression until aTc is present in the culture (Figure 1A) (41, 42). To combine the Bxb1 integrase
112 system with DiCre, we first introduced a DiCre expression cassette at the benign *pfs47* locus (27)
113 in the *P. falciparum* NF54^{attB} strain (43) (Figure S1) and then integrated the mNG-knockER
114 reporter construct at the *attB* site in the *cg6* locus on chromosome 6 (43) in this NF54$^{attB:DiCre}$ line.
115 Upon treatment with rapamycin, parasites efficiently excised the knockER cassette (kER),
116 resulting in the expected tag switching from FLAG to HA (Figure 1B,C). Examination of untreated
117 parasites by live microscopy showed a peripheral mNG signal, consistent with secretion to the

118 PV (Figure 1D). In contrast, following treatment with rapamycin the mNG signal was dramatically
119 altered to an intracellular, perinuclear pattern that co-localized with ER Tracker, confirming
120 retention in the ER (Figure 1D). To determine the level of ER retention achieved by KDEL fusion,
121 we quantified the distribution of mNG fluorescence between the parasite periphery (PV) and
122 interior and observed substantial re-localization following KDEL fusion, indicating robust retrieval
123 by ERD2 (Figure 1E, mean internal mNG 42.54 ± 6.0% in DMSO vs 84.66 ± 6.9% in Rap).
124 Importantly, ER retention of mNG had no impact on parasite growth (Figure 1F) showing that
125 knockER can successfully retrieve a secreted reporter to the ER without impacting parasite
126 fitness.
127

128 **knockER reveals Golgi-dependent trafficking and essential apicoplast functionality of**
129 **ClpB1**

130 Next, we applied knockER to an endogenous gene for conditional loss-of-function
131 mutagenesis. We choose ClpB1, a poorly characterized, nuclear-encoded AAA+ class 1
132 Clp/HSP100 chaperone that is targeted to the apicoplast (44, 45). As apicoplast ablation can be
133 chemically rescued with isopentenyl pyrophosphate (IPP) (46), we reasoned that IPP
134 supplementation would provide a simple validation that any loss of parasite fitness is a direct
135 effect of sequestering ClpB1 away from its site of action and not an indirect result of ER stress.
136 ClpB1 contains both a signal peptide for ER entry and a transit peptide for apicoplast targeting
137 and localization of ClpB1 to this organelle was previously confirmed by both microscopy and
138 proteomic analyses (36, 45). Using CRISPR/Cas9 editing, we fused mNG to the C-terminus of
139 ClpB1 followed by the kER cassette (Figure 2A). As expected, IFA demonstrated co-localization
140 with the apicoplast marker ACP1, confirming ClpB1 localization to this organelle (Figure 2B).
141 Treatment with rapamycin resulted in efficient excision (Figure 2C) and switching to the 3xHA-
142 KDEL tag produced a shift in migration by Western blot consistent with an increase in molecular
143 weight of ~14 kDa in the rapamycin treated samples, indicating that the N-terminal transit peptide

144 (residues 24-152, 13.9 kDa) is no longer cleaved in the ClpB1-KDEL fusion (Figure 2D). Since
145 this maturation event takes place in the apicoplast (47), this suggested that ClpB1 was no longer
146 being trafficked to this organelle. Indeed, live microscopy showed a dramatic re-localization of
147 mNG from puncta to a perinuclear distribution that co-localized with ER Tracker, indicative of
148 successful ER retrieval (Figure 2E).

149 While its functional importance has not been directly tested, ClpB1 is expected to be
150 essential for blood-stage survival based on saturating insertional mutagenesis in *P. falciparum*
151 and pooled knockout screens in *P. berghei* (48, 49). Indeed, ER retention of ClpB1 was lethal and
152 resulted in delayed parasite death (Figure 2F), consistent with an essential role in the apicoplast
153 (50, 51). Moreover, supplementation with IPP fully rescued parasite growth, confirming the
154 observed phenotype was apicoplast-specific and not due to a disruption of ER homeostasis
155 following ClpB1 retention (Figure 2F). Rapamycin-treated parasites supplemented with IPP
156 showed dispersed, vesicular ACP1 signal consistent with plastid disruption, further indicating
157 ClpB1 is required for apicoplast maintenance (Figure 2G). Taken together, these results show for
158 the first time that ClpB1 is an indispensable component of the apicoplast machinery and illustrate
159 that knockER can be used for protein loss-of-function studies in *P. falciparum*.

160

161 **knockER induces ER retrieval of rhoptry proteins**

162 Having demonstrated that knockER is suitable to generate loss-of-function phenotypes by
163 protein mis-localization to the ER, we next tested this knock sideways approach on an expanded
164 set of endogenous soluble and membrane proteins that traffic through the secretory pathway to
165 diverse destinations, including secretory organelles and the PV/PVM. We began by attempting to
166 retrieve RON6, a soluble rhoptry-neck protein that is injected into the PV during invasion. Attempts
167 predating CRISPR technology to disrupt *Pfron6* or truncate its Cysteine-rich C-terminus were
168 unsuccessful (52). More recently, saturating transposon mutagenesis in *P. falciparum* recovered
169 a single insertion within an intron (48) expected to generate a truncation at residue 713 of 950,

170 leaving most of the protein intact (Figure 3A). Curiously, RON6 orthologs in rodent malaria
171 parasites lack the cysteine-rich region which accounts for the C-terminal ~23% of *P. falciparum*
172 RON6, roughly corresponding to the truncated region in the insertional mutant. As RON6 was not
173 targeted in the PlasmoGEM data set, its suspected essentiality remains uncertain (49). To directly
174 test the importance of RON6, we generated RON6-kER parasites, which underwent efficient
175 excision upon rapamycin treatment (Figure 3B). Rapamycin treatment resulted in re-localization
176 of RON6 from the rhoptries to the ER and produced a minor but reproducible growth defect (Figure
177 3C,D). These results suggest that RON6 is dispensable in the blood stage, although we cannot
178 exclude the possibility that small amounts of RON6-KDEL may escape ERD2 surveillance at
179 levels sufficient to mediate a critical function. Additionally, the minor fitness defect that results
180 from RON6-KDEL fusion could be the indirect result of modest ER stress induced by RON6
181 retention. Nonetheless, these findings clearly demonstrate that knockER efficiently retrieves
182 secretory proteins synthesized during the brief period of merozoite formation at the terminal phase
183 of intraerythrocytic development.
184

185 **ER retention of EXP2 produces a lethal defect independent to loss of PVM transport**
186 **function**

187 Having successfully retained several soluble proteins in the ER using knockER, we next
188 tested conditional retrieval of a membrane protein. Solute permeation across the PVM is mediated
189 by a nutrient-permeable channel (53, 54) whose identity was recently tied to EXP2, a PVM protein
190 broadly conserved among vacuole-dwelling apicomplexans (55, 56). EXP2 contains a signal
191 peptide followed by an N-terminal amphipathic helix and oligomerizes to form a heptameric pore
192 in the PVM (26, 57, 58). It is currently unknown how pore formation is specifically constrained to
193 the PVM to avoid perforating other membranes along the secretory pathway or the parasite
194 plasma membrane. While not structurally homologous to the EXP2 pore, bacterial α-helical pore
195 forming toxins are functionally analogous and provide a possible model for EXP2 pore formation.

196 These proteins are typically maintained in a monomeric state that shields a membrane-spanning
197 amphipathic helix, enabling soluble trafficking until contact with components of a target membrane
198 triggers conformational rearrangement, leading to membrane insertion and oligomerization (59).
199 If EXP2 traffics in a similar configuration, then its C-terminus will enter the secretory
200 pathway lumen and be sensitive to ER-retrieval by KDEL fusion. Indeed, we endogenously tagged
201 EXP2 with a version of the kER cassette lacking mNG and found that KDEL fusion disrupted
202 EXP2 trafficking to the PV and resulted in ER retention, confirming its C-terminus resides in the
203 secretory pathway lumen (Figure 4A-D and S2). Notably, ER retrieval of EXP2 caused rapid
204 parasite death at earlier time points than post-transcriptional conditional knockdown of EXP2 (55,
205 60) (Figure 4E). To test whether this was solely due to loss of EXP2 transport functions in the PV
206 and not an indirect result of retaining EXP2 in the ER, we generated parasites expressing a
207 second copy of EXP2-mNG-kER from the *attB* locus under the control of its own promoter, leaving
208 the endogenous EXP2 locus unaltered (Figure S2). Retrieval of this second copy of EXP2 to the
209 ER also resulted in parasite death, indicating that EXP2 retention in the ER is toxic independent
210 of compromised transport functions at the PVM (Figure 4F,G). In contrast, ER retrieval of a second
211 copy of EXP2 lacking the amphipathic helix rescued parasite death (Figure 4H,I and S2). As
212 expected, prior to KDEL fusion the ΔTM version of EXP2 localized to the PV and the digestive
213 vacuole (due to endocytosis of PV proteins along with RBC cytosol); surprisingly, however, some
214 cells also showed EXP2ΔTM-mNG export into the RBC cytoplasm (arrow, Figure 4H). The
215 requirement for the amphipathic helix in EXP2-kER toxicity suggests that increasing EXP2 dwell
216 time in the early secretory pathway may trigger an unfolded protein response or cause aberrant
217 EXP2 pore formation in the ER membrane. Thus, this may provide a new tool for studying EXP2
218 pore formation but also indicates knockER may not be appropriate for loss-of-function studies of
219 certain membrane proteins.
220
221 **ER retention of PTEX150 but not HSP101 results in loss of PTEX function *in vitro***

222 In malaria parasites, the nutrient-permeable channel has been additionally functionalized
223 by the flange-like adaptor PTEX150 which docks the AAA+ chaperone HSP101 onto EXP2 to
224 form the *Plasmodium* Translocon of Exported proteins (PTEX), transforming EXP2 into a protein-
225 conducting pore to translocate effector proteins across the PVM and into the erythrocyte (24-26,
226 55, 61). Interestingly, HSP101 shows a dual localization to both the PV and the ER as opposed
227 to EXP2 and PTEX150, which localize exclusively to the PV and can form a sub-complex
228 independent of HSP101 (23, 38, 62, 63). We verified this unique ER localization of HSP101 by
229 protease protection assays in parasite lines expressing fluorescently tagged versions of each
230 PTEX core component, confirming an internal, perinuclear pool of HSP101 but not EXP2 or
231 PTEX150 (Figure S3). This arrangement suggests that in addition to powering translocation in
232 the assembled PTEX complex, HSP101 may also function upstream of the vacuole, possibly
233 initiating cargo selection early in the secretory pathway (23). While several HSP101 conditional
234 knockdown (23, 25) or inactivation (24) strategies have demonstrated an essential role in protein
235 export, it is difficult to resolve distinct compartmental functions with these mutants given that they
236 impact the total protein pool and have no sub-compartmental resolution. In contrast, knockER
237 provides a strategy to resolve potential HSP101 functions across distinct compartments by
238 redistributing the target protein pool from the PV to the ER.

239 In an attempt to separate HSP101 ER function from its role in the PV, we generated a kER
240 fusion to the endogenous copy of HSP101. In parallel, we also generated a PTEX150-kER line,
241 reasoning that since HSP101 and PTEX150 have similar expression timing/levels and are
242 exclusively involved in protein export but not nutrient uptake (55), PTEX150 would provide a
243 control for knockER inactivation of PTEX activity independent of ER function. As expected, the
244 PTEX150-KDEL fusion was efficiently retrieved to the ER, producing a lethal growth defect and
245 accompanying block in protein export (Figure 5A-E), similar to *glmS* ribozyme-mediated
246 knockdown of PTEX150 (25). Importantly, ER retention of a second copy of PTEX150-kER in
247 parasites where the endogenous PTEX150 locus was unmodified did not impact growth,

248 demonstrating that the phenotype observed upon ER retention of the endogenously tagged
249 protein is a direct result of functional disruption of PTEX150 (Figure S4A-D).

250 Prior to knockER induction, HSP101-mNG-3xFLAG showed a small but significantly more
251 internal distribution than PTEX150-mNG-3xFLAG, consistent with the unique HSP101 ER pool
252 (Figure S4E, 24 hrs post DMSO treatment: 39.41±11.00% internal HSP101 vs 35.58±7.41%
253 internal PTEX150, P = 0.0024, unpaired t test). Unexpectedly, although the rapamycin-induced
254 HSP101-KDEL fusion increased ER localization similar to PTEX150 (Figure 5F-H), parasite
255 growth was completely unaffected and protein export was not detectibly impacted (Figure 5I,J),
256 sharply contrasting with the lethal export defect observed with HSP101 depletion or inactivation
257 mutants (23-25). Indeed, HSP101-kER parasites could be cultured indefinitely following excision
258 and displayed sustained ER retention of HSP101 (Figure 5H and S4E,F, mean Rap internal
259 HSP101 58.82±9.58% at 24 hours vs 54.82±9.84% at 7 days). As an orthogonal approach to
260 monitor protein redistribution by KDEL fusion, we released infected RBCs with saponin to
261 permeabilize the PVM and quantified fluorescence via flow cytometry with or without proteinase
262 K treatment. Again, we observed an increase in protected fluorescence following rapamycin
263 treatment, consistent with redistribution of HSP101 to the ER (Figure S5A). Importantly, PCR and
264 Western blot indicated that rapamycin-treated parasites had undergone complete excision with
265 the pre-excised FLAG-tagged version of HSP101 no longer detectible (Figure 5F,G).
266 Furthermore, both the mNG-FLAG and mNG-HA-KDEL tagged versions of HSP101 migrated as
267 a single band at the expected size for the full-length fusion proteins with no apparent breakdown
268 products, ensuring that the mNG signal distribution observed by live microscopy reflected an
269 intact HSP101 fusion (Figure 5G, S5C and S7B).

270 While a large fraction of PTEX150 and HSP101 was clearly ER-retained following
271 knockER induction, some peripheral signal was still apparent after rapamycin treatment (Figure
272 5C,H). To determine whether the observed phenotypic differences between HSP101 and

273 PTEX150 were due to a difference in sensitivity to ERD2 surveillance, we quantified the internal
274 mNG fluorescence signal in HSP101- and PTEX150-kER parasites following KDEL fusion. In
275 synchronized parasites, a similar increase in internal signal was observed in both lines at 24 hours
276 post Rap treatment (Figure S4E, mean Rap internal HSP101 58.82±9.58% vs 56.32±18.56% for
277 PTEX150). Since a comparison could not be made with PTEX150-kER parasites at 7 days due
278 to parasite death by the second cycle follow excision, we compared HSP101-kER parasites with
279 PTEX150-kER^{attB} control parasites 7 days after excision and again observed a comparable
280 internal signal redistribution (Figure S4F, mean Rap internal HSP101 54.82±9.84% vs
281 61.75±16.27% for PTEX150 at 7 days). As differential ER retrieval cannot account for parasite
282 insensitivity to HSP101-kER, these results indicate vacuolar HSP101 levels are uniquely
283 maintained in excess from what is required for PTEX function at the PVM.

284 To determine the amount of HSP101 need to support parasite growth, we combined
285 knockER with the TetR-DOZI-aptamers system to generate a HSP101-kER line that also allows
286 for titration of HSP101 expression with aTc (Figure 6A). Like the original HSP101-kER line,
287 rapamycin-treated HSP101-kER$^{TetR\text{-}DOZI}$ parasites exhibited ER retention of HSP101 without
288 impacting parasite growth or export of representative PEXEL and PNEP proteins (Figure 6B-D).
289 However, HSP101 depletion following aTc washout resulted in a robust block in protein export
290 and parasite death (Figure 6D and S5B,C), consistent with previous HSP101 knockdown or
291 inactivation studies (23-25). To determine the level of total HSP101 reduction sufficient to impact
292 growth, we grew synchronized parasites at a range of aTc concentrations following DMSO or
293 rapamycin treatment and measured mNG fluorescence via flow cytometry in parallel with parasite
294 growth (Figure 6E,F). Interestingly, rapamycin-treated parasites displayed a small but
295 reproducible increase in total HSP101, consistent with a reduction in HSP101 turnover by
296 endocytosis from the PV to the digestive vacuole following redistribution to the ER (Figure 6E).
297 More importantly, we determined that a ~70% reduction in total HSP101 levels was necessary to

298 impact parasite growth, showing that a relatively small amount of HSP101 is needed for survival
299 *in vitro* (Figure 6E,F, 5 nM aTc), suggesting that redistribution of HSP101 by knockER does not
300 meet the threshold required to impact HSP101 PV function and parasite fitness.

301 If HSP101 functions exclusively in the PV, then knockER-mediated depletion of vacuolar
302 HSP101 levels should hypersensitize parasites to HSP101 knockdown. To test this, we measured
303 the dose-response to aTc in DMSO- or rapamycin-treated parasites and strikingly observed no
304 shift in the EC50, indicating substantial redistribution of HSP101 from the PV to the ER does not
305 hypersensitize parasites to HSP101 knockdown (Figure 6G). This suggests that the PV-localized
306 function of HSP101 does not fully account for its role in parasite fitness, implying a distinct
307 important role in the ER. Taken together, our results provide the first functional genetic evidence
308 for an extra-vacuolar function of HSP101, consistent with the revised model of protein export (23).
309

310 **ER retention of HSP101 is lethal *in vivo***

311 Lack of observable phenotypes *in vitro* can sometimes be masked by the rich resources
312 available in culturing conditions (64, 65). In addition, exported effectors critical for survival in the
313 vertebrate host may be dispensable in culture (11). Indeed, export-related defects that escape
314 detection *in vitro* can be exposed *in vivo* where parasites have to contend with host defenses and
315 more limited nutrient access (66, 67). To expose any impact on export by ER retention of HSP101
316 masked during *in vitro* culture, we tagged HSP101 and PTEX150 with kER in a *P. berghei* rodent
317 malaria DiCre parasite and evaluated the impact of ER retrieval on parasite survival during mouse
318 infection (Figure S6A). Similar to *P. falciparum* knockER mutants, rapamycin treatment *ex vivo*
319 produced efficient excision and ER retrieval of PbPTEX150 and PbHSP101 (Figure 6A-D). After
320 overnight *ex vivo* culture to allow for tag switching, equal numbers of DMSO or rapamycin treated
321 parasites were IV injected into naïve mice. Strikingly, while DMSO controls became patent by day
322 two post-injection, neither KDEL-fused PbPTEX150 or PbHSP101 parasites appeared over the
323 course of 10 days before the experiment was terminated (Figure 7E,F and S6B). That ER-retrieval

324 of PbHSP101 compromises function sufficiently to prohibit survival in the mammalian host
325 reinforces the critical role of HSP101 in the PV and indicates that KDEL-mediated depletion of
326 HSP101 from the *P. falciparum* PV does not sufficiently reduce PTEX activity to impact parasite
327 fitness under less taxing *in vitro* culture conditions. Collectively, these results provide support for
328 a distinct HSP101 activity in the ER upstream of its function in PVM translocation at the assembled
329 PTEX complex.
330
331 **Discussion**
332 Several genetic tools are now available for protein loss-of-function studies in *Plasmodium*
333 *spp.* (68), including knock sideways for conditional sequestration of a target protein away from its
334 normal site of function (69). While this system is not currently amenable to parasite proteins that
335 enter the secretory pathway, conditional control of secretory traffic has been achieved in *P.*
336 *falciparum* by ligand-mediated alteration of the N-terminal transit peptide that controls apicoplast
337 targeting, enabling redirection of plastid proteins into the default secretory pathway (70).
338 Additionally, conditional ER release systems have been developed in model eukaryotes based
339 on ER retrieval machinery (71). In contrast, knockER provides a simple, DiCre-mediated knock
340 sideways strategy that exploits the ERD2/KDEL receptor (KDELR) system for conditional ER
341 retrieval, providing a generalizable approach for interrogating secreted proteins in genetically
342 tractable eukaryotes.
343 In this study, we demonstrate knockER can be used for trafficking and loss-of-function
344 studies. The ability to determine whether a protein traffics from the ER through the *cis* Golgi is an
345 important consideration for nuclear-encoded apicoplast proteins where Golgi-dependent and -
346 independent trafficking routes have been reported (33, 35, 72). While these apicoplast trafficking
347 studies were carried out with reporters and chimeras, knockER allows for monitoring *cis* Golgi
348 transit of endogenous proteins. The sensitivity of ClpB1 to KDEL-mediated ER retrieval
349 demonstrates a Golgi-dependent trafficking route to the apicoplast. Moreover, we show for the

350 first time that this AAA+ chaperone essential for apicoplast maintenance. ClpB1 is one of four
351 Clp/HSP100 chaperones encoded by *Plasmodium spp*., three of which localize to the parasite
352 plastid while the fourth, HSP101 (previously known as ClpB2) localizes to the PV and ER (45).
353 The other apicoplast-targeted members of this quartet in include the nuclear-encoded ClpC, which
354 mediates regulated proteolysis together with the serine protease ClpP (73, 74), and ClpM, now
355 the only uncharacterized member of this group and one of the few proteins encoded on the
356 apicoplast genome. Similar to the well-studied function of its closest orthologs (75), ClpB1 likely
357 acts as a disaggregase that, together with ClpC/P and ClpM, forms a critical proteostasis system
358 required to maintain and regulate the apicoplast proteome (76).

359 ER perturbations can trigger an integrated stress response leading to cell arrest or death
360 (77, 78). *Plasmodium* possesses one of the widely conserved ER stress sensors, the PERK-
361 eIF2α pathway which halts protein translation and flux through the secretory pathway (19, 29, 79-
362 81), and knockER experiments should be controlled for indirect effects. Importantly, conditional
363 ER retrieval of proteins produced from their endogenous locus or by heterologous expression was
364 not generally toxic, enabling loss-of-function studies with knockER. The single notable exception
365 was EXP2, which rapidly killed parasites when retained in the ER independent to loss of its PVM
366 transport function. EXP2-KDEL toxicity was dependent on the amphipathic helix that forms the
367 membrane-spanning region in the oligomeric EXP2 pore (26), suggesting that accumulation of
368 EXP2 in the ER might trigger an unfolded protein response or lead to premature pore formation
369 in the early secretory pathway. More work is required to determine if this outcome is specific to
370 EXP2 or a general problem for unnatural ER-retrieval of membrane proteins. Indirect fitness
371 defects aside, retrieval of EXP2-KDEL demonstrates that its C-terminus enters the secretory
372 pathway lumen, consistent with a soluble EXP2 trafficking state that precedes membrane
373 integration at the PVM. Regardless of the basis for EXP2-kER toxicity, these experiments
374 highlight that knockER can also be used to investigate membrane topology. While ER-resident
375 type I membrane proteins utilize a different mechanism for retrieval as their C-termini face the

376 cytosol of the cell (82, 83), ERD2/KDELR can retrieve membrane proteins whose C-termini face
377 the lumen (84) and thus knockER should be able to distinguish the topology of single and multi-
378 pass transmembrane domain-containing proteins.

379 A unique feature of knockER is the ability to redistribute secreted proteins from their
380 terminal destination to the ER, providing a method to resolve potential HSP101 functions between
381 the PV and ER. We tagged both HSP101 and the translocon adaptor PTEX150 with knockER,
382 reasoning that ER retrieval of either protein would produce a lethal export defect but that
383 differential impacts on exported cargo trafficking might be exposed. Unexpectedly, ER retrieval of
384 HSP101 had no impact on *P. falciparum* growth or export of representative PEXEL and PNEP
385 proteins *in vitro*. Similar PV depletion of PTEX150 produced the anticipated lethal export block,
386 revealing that HSP101 PV levels are uniquely maintained in excess. As a AAA+ ATPase, HSP101
387 is the only enzyme in the PTEX core complex and its activity may exceed what is required to
388 support parasite fitness in the less demanding *in vitro* culture environment, as previously seen for
389 the aspartic protease Plasmepsin 5 that licenses proteins for export in the ER (30, 85). Indeed,
390 while critical to avoiding host defenses *in vivo*, most exported proteins are dispensable during *in*
391 *vitro* culture (11). Not surprisingly, ER retrieval of *P. berghei* HSP101 abolished parasite survival
392 in the mouse host, reinforcing the established PV function of HSP101 in effector translocation at
393 the PVM. In contrast, depletion of HSP101 PV levels in cultured *P. falciparum* likely impacts
394 translocon kinetics or export of specific proteins in ways that are not problematic for growth *in*
395 *vitro* and thus difficult to detect.

396 Intriguingly, redistribution of HSP101 from the PV to the ER did not hypersensitize
397 parasites to HSP101 knockdown, suggesting that the PV-localized function of HSP101 does not
398 fully account for its contribution to parasite fitness. These results provide support for an important,
399 additional HSP101 function upstream of the PV, presumably in cargo recognition at the ER and/or
400 guiding export-destine proteins to PTEX, as recently proposed (23). Future work dissecting the
401 specific extra-vacuolar role(s) of HSP101 may resolve the long-standing question of how early

402 events in this pathway that mark proteins for export, such as PEXEL processing during ER entry,
403 are connected to cargo recognition and ultimate PVM translocation into the host cell at the
404 assembled PTEX complex.
405
406 **Methods**
407 **Parasite culture.** *P. falciparum* NF54$^{attB\text{-}DiCre}$ and derivatives were cultured in RPMI 1640 medium
408 supplemented with 27 mM sodium bicarbonate, 11 mM glucose, 0.37 mM hypoxanthine, 10 µg/ml
409 gentamicin and 0.5% Albumax I (Gibco). Parasites were maintained in deidentified, Institutional
410 Review Board-exempt RBCs obtained from the American National Red Cross. *P. berghei* ANKA
411 clone 2.34 and derivatives were maintained in Swiss Webster mice (Charles River). All
412 experiments involving rodents were reviewed and approved by the Iowa State University
413 Institutional Animal Care and Use Committee.
414
415 **Plasmids and genetic modification of *P. falciparum* and *P. berghei*.** All cloning was carried
416 out with NEBuilder HIFI DNA (NEB). Primer sequences are given in Table S1. To generate
417 NF54$^{attB\text{-}DiCre}$ parasites, a DiCre expression cassette was inserted into the *pfs47* gene in NF54^{attB}
418 parasites (43) using a marker-free CRISPR/Cas9 editing strategy as described (27). Loss of the
419 endogenous *pfs47* locus was monitored with primers P1/2 and P3/4 and integration was
420 confirmed using primers P1/5 and P6/4. To confirm DiCre activity in this line, a loxP-flanked mNG
421 coding sequence with a 3xHA tag was PCR amplified using primers P19/20 and inserted between
422 AvrII and AflII in pLN-ENR-GFP cite (86), resulting in the plasmid JRB416. This plasmid was co-
423 transfected with pINT (86) into NF54$^{attB\text{-}DiCre}$ parasites and selected for with 2.5 µg/ml blasticidin-
424 S (BSD) 24-48hrs post-transfection.
425 To generate the kER fusion cassette, homology flanks targeting the 3' end of *exp2* were
426 amplified from pyPM2GT-EXP2-3xHA-GFP11 (55) using P21/22 and inserted between XhoI and
427 AvrII in pPM2GT-HSP101-3xFLAG (55). The loxPint sequence (87) was amplified with P23/24

428 and inserted immediately upstream of the 3xFLAG tag at AvrII in this vector. A partial loxPint
429 containing the loxP sequence and 3' portion of the intron followed by a 3xHA-KDEL tag was then
430 amplified with P25/26 and inserted into EagI, resulting in the plasmid JRB492. Finally, the mNG
431 coding sequencing was amplified from pyPM2GT-EXP2-mNG (88) with P27/28 and inserted into
432 AvrII in JRB492, resulting in plasmid JRB508.

433 To generate the SP-mNG-kER reporter, the *exp2* promoter and signal peptide were
434 amplified from parasite genomic DNA with P29/30 and the mNG-KER cassette was amplified from
435 JRB508 with P31/32 and these amplicons were assembled together in a second PCR reaction
436 with P29/32 and inserted into AscI/ApaI in pKD (42), resulting in the plasmid JRB543. For
437 expression of a second copy of EXP2-kER from the attB locus, the *exp2* promoter and full-length
438 gene were amplified from genomic DNA with P29/33 and inserted between AscI/BamHI in
439 JRB543, resulting in the plasmid JRB526. For expression of a second copy of EXP2-kER lacking
440 the amphipathic helix, a recoded portion of the *exp2* coding sequence beginning immediately after
441 the amphipathic helix (codon 72) was amplified from pEXP2^{apt} (55) and inserted at BamHI in
442 JRB543, resulting in the plasmid JRB544. These plasmids were each co-transfected with pINT
443 and selected with 2.5 µg/ml blasticidin-S as described above. To relieve translational repression
444 by TetR-DOZI, parasite cultures were supplemented with 500 nM aTc.

445 For generation of ClpB1-kER and RON6-kER lines, a Cas9 gRNA target was chosen just
446 downstream (*clpB1*, ATTTTTAGAAAAATATTATG) or just upstream (*ron6*,
447 TAATACATACAACGTACCAA) of the stop codon and the gRNA seed sequences were
448 synthesized as primers P34 and P35, respectively, and inserted into the AflII site of pAIO3 (38),
449 resulting in plasmids JRB143 and MAF22, respectively. To target the 3' end of clpB1 or ron6, a 5'
450 homology flank (up to but not including the stop codon) was amplified from genomic DNA using
451 P36/37 or P38/39, incorporating synonymous shield mutations in the gRNA target sites. A 3'
452 homology flank was amplified using P40/41 or P42/43. The corresponding 5' and 3' flank
453 amplicons were assembled in a second PCR reaction using P40/37 and P42/39 and inserted

454 between XhoI/AvrII in JRB508, resulting in plasmids MAF20 and MAF27, respectively. These
455 plasmids were linearized with AflII and co-transfected with the corresponding Cas9/gRNA plasmid
456 into NF54$^{attB\text{-}DiCre}$. Selection was applied with 5 nM WR99120 24 hrs post-transfection and clonal
457 lines were isolated by limiting dilution after parasites returned from selection.

458 For generation of PTEX150-kER and HSP101-kER lines, flank assemblies targeting the
459 3' end of each gene were amplified using P44/45 from pyPM2GT-PTEX150-3xHA-GFP11 (55) or
460 P46/47 from pyPM2GT-HSP101-3xHA-GFP11 (55) and inserted between XhoI/AvrII in JRB508,
461 resulting in plasmids MAF16 and MAF17, respectively. These plasmids were linearized with AflII
462 and co-transfected with pAIO-PTEX150-CT-gRNA or pAIO-HSP101-CT-gRNA (55), selected with
463 5 nM WR99120 and cloned after parasites returned. For generation of EXP2-kER line, plasmid
464 JRB492 was linearized and co-transfected with pUF-Cas9-EXP2-CT-gRNA (55) and selected
465 with 5 nM WR99120. For generation of HSP101-kER$^{TetR\text{-}DOZI}$ lines, flank assembles were amplified
466 using P48/49 and inserted between AscI/BamHI in JRB526, resulting in plasmid MAF41. This
467 plasmid was linearized with AflII and co-transfected with pAIO-HSP101-CT-gRNA, selected with
468 2.5 µg/ml blasticidin-S and 500nM aTc, and cloned after parasites returned.

469 For expression of a second copy of PTEX150-kER from the *attB* locus, the *ptex150*
470 promoter and full-length gene were amplified from genomic DNA with P50/51 and the mNG-KER
471 cassette was amplified from JRB508 with P52/53. These amplicons were assembled together in
472 a second PCR reaction using P50/53 and inserted between ApaI/AflII in pLN-ENR-GFP (86),
473 resulting in the plasmid MAF39. This plasmid was co-transfected with pINT, selected with 2.5
474 µg/ml blasticidin-S and parasites were cloned after returning.

475 To generate the line bearing endogenous EXP2-mRuby and HSP101-mNG tags, the
476 plasmid pbEXP2-mRuby3 (89) was first linearized with AflII and co-transfected with pUF-Cas9-
477 EXP2-CT-gRNA (55) into NF54$^{attB:DiCre}$. Selection was applied with 2.5 µg/ml blasticidin-S. Next,
478 the mNG coding sequence was amplified using P54/55 and inserted between AvrII/EagI in
479 pPM2GT-HSP101-3xFLAG (55) to replace the FLAG tag with mNG, resulting in the plasmid

480 JRB325. This plasmid was linearized with AflII and co-transfected with pAIO-HSP101-CT-gRNA
481 (89) into the NF54$^{attB:DiCre}$::EXP2-mRuby parasites. Selection was applied with 5nM WR99120
482 resulting in the line NF54$^{attB:DiCre}$::EXP2-mRuby+HSP101-mNG.

483 For generation of PTEX150-kER and HSP101-kER lines in *P. berghei*, the plasmid pBAT
484 (90) was digested with MluI/XhoI and the primer P56 was used as an insert to remove the
485 intervening AvrII, SnaBI and XhoI sites from the MCS. Next, the mRuby3 coding sequence fused
486 to the PbEXP2 signal peptide was amplified with P57/58 and inserted between SwaI/BamHI,
487 replacing the GFP. The mNG-kER tagging sequence was amplified from plasmid JRB508 using
488 P59/60 and inserted between SacII/SphI, replacing the mCherry-3xMYC. Finally, 5' flanks to tag
489 *P. berghei hsp101* or *ptex150* with mNG-kER were amplified from *P. berghei* genomic DNA using
490 P61/62 or P63/64, respectively, and 3' flanks were amplified using P65/66 or P67/68, respectively.
491 The corresponding 5' and 3' flank amplicons were assembled with an intervening AflII site in a
492 second PCR reaction using P65/62 or P67/64, respectively, and inserted at SacII, resulting in
493 plasmids pPbHSP101-kER and pPbPTEX150-kER. The plasmids were linearized at AflII and
494 transfected as described (91) into the marker-free HP DiCre line (92). Transfected parasites were
495 reinjected into naïve mice and selection was applied with 0.07 mg/ml pyrimethamine in drinking
496 water provided *ad libitum* 24 hours later. After returning from selection, transfected populations
497 were cloned by limiting dilution IV injection into naïve mice to generate isogenic populations
498 designated PbHSP101-kER and PbPTEX150-kER.

499

500 ***P. falciparum* growth assays**. Growth assays were done as described previously (93). Briefly,
501 parasites were treated with either DMSO or 10nM rapamycin for 3hrs and washed 1X. Then,
502 parasites were seeded between 0.2-1% parasitemia in triplicate and monitored every 48hrs by
503 flow cytometry on an Attune NxT (ThermoFisher) by nucleic acid staining with PBS containing 0.8
504 µg/ml acridine orange. For IPP rescue experiments, ClpB1-kER cultures were supplemented with
505 200µM IPP. For kER fusions expressed from the *attB* locus, cultures were supplemented with

506 1μM aTc 24hrs prior to rapamycin treatment to relieve TetR-DOZI-aptamer translational
507 repression. For HSP101-kER$^{TetR-DOZI}$ parasites, aTc was removed by washing parasites 7X with
508 13mL of BSD only media. 500nM aTc was then supplemented back to control parasites. As
509 required, parasites were sub-cultured to avoid high parasite density, and relative parasitemia at
510 each time point was back-calculated based on actual parasitemia multiplied by the relevant
511 dilution factors. Data were modeled using Prism 9 (GraphPad Software).

512 For EC_{50} shift assays, parasites were treated with DMSO or rapamycin before removal of
513 aTc. After aTc removal, parasites were seeded at 0.5% parasitemia with 2-fold dilutions of aTc
514 starting from 500nM, in triplicate and parasite growth was monitored after 72hrs.

515

516 ***P. berghei* kER experiments.** Parasite-infected blood was collected by cardiac puncture and
517 cultured in RPMI supplemented with 20% FBS. Cultures at 3-4% were treated with 10 nM
518 rapamycin or DMSO for 3-4 hours followed by a media change. After 18 hours of additional
519 culture, parasites were harvested for diagnostic PCR, live fluorescence microscopy and Western
520 blot. Equal numbers of DMSO or rapamycin-treated infected RBCs (~10,000 parasites per
521 injection) were IV injected into naïve mice and parasitemia was monitored by giemsa-stained
522 blood smear every two days.

523

524 **Microscopy.** For live microscopy, *P. falciparum* parasites were treated with either DMSO or 10nM
525 rapamycin and viewed 24-48hrs later. Hoescht (33342, Invitrogen; 1:10,000) was used for to
526 visualize the nucleus by incubating with parasites 2-5min prior to visualization. ER-Tracker Red
527 (Invitrogen; 1:1000) was used to visualize the ER by incubating with parasites 30min at 37°C prior
528 to visualization. For constructs expressed using the *attB* locus, parasites were grown in 1μM aTc
529 for 24hrs prior to incubation with DMSO or Rap to allow expression of the constructs. For *P.*
530 *berghei*, parasites were isolated via cardiac puncture, treated with DMSO or rapamycin for 3hrs,
531 and allowed to develop overnight in culture before visualization. Quantification of MFI was

532 calculated using the measured Integrated Density value from Fiji (94). The internal MFI was
533 calculated using an ROI within the parasite PV and subtracting that from the whole parasite MFI
534 using an ROI outside the PV boundary. The percent MFI was then calculated by dividing the
535 internal MFI by the whole parasite MFI.

536 For protease protection assays of live cells, parasites were treated with 0.03% Saponin in
537 1X PBS for 15min at 4°C. Purified parasites where then washed once with 5mL of 1X PBS and
538 once with 5mL of digestion buffer (50mM Tris pH 7.5, 150mM NaCl, 1mM $CaCl_2$) (23). Parasite
539 samples where then split into two identical tubes, one of which was treated with 20µg/mL of
540 Proteinase K (740506.75, Macherey-Nagel), and incubated at 37°C for 15min. Proteinase K was
541 removed and samples resuspended with digestion buffer plus protease inhibitor cocktail (Halt
542 78429, Thermo Scientific) before visualization.

543 For IFAs of the EXP2- and ClpB1-kER lines, parasites were treated with either DMSO or
544 10nM rapamycin and fixed 24hrs or 144hrs later as described previously (93). For HSP101-
545 $kER^{TetR\text{-}DOZI}$ lines, parasites were synchronized with 5% sorbitol, treated with either DMSO or
546 10nM rapamycin, grown with or without 500nM aTc, and fixed 48hrs later. Briefly, parasites were
547 fixed with Fixative Solution (4% paraformaldehyde, 0.0075% glutaraldehyde in PBS) for 25min at
548 room temperature in the dark. Parasites were then permeabilized with 0.1% Triton in PBS for 10
549 minutes at room temperature while rocking. Parasites were washed 1X with PBS and then
550 blocked with 3% BSA in PBS for 1hr at room temperature. Primary antibody was applied in 3%
551 BSA solution for 1hr at room temperature, washed 2X with PBS, followed by secondary antibody
552 incubation for 1hr at room temperature. After 2X washes with PBS, parasites were adhered onto
553 Poly-L-lysine covered coverslips and then mounted onto slides. For parasites probed with SBP1,
554 parasites were acetone fixed as in (38). Briefly, thin smears were immersed in 100% acetone for
555 2min. Smears were washed 1X with PBS and then blocked with 3% BSA in PBS for 1hr at room
556 temperature. Primary antibody was applied in 3% BSA solution for 1hr at room temperature,
557 washed 2X with PBS, followed by secondary antibody incubation for 1hr at room temperature.

558 After 2X washes with PBS, slides were mounted with DAPI, covered with a coverslip and sealed.
559 The antibodies used for IFA were: mouse anti-HA antibody (clone 16B12; BioLegend, 1:200 IFA
560 and WB), rabbit polyclonal anti-HA SG77 (ThermoFisher; 1:500 IFA and WB), rabbit anti-
561 PfGRP78 (BiP) (MRA-1246; BEI Resources, NIAID, NIH 1:100), mouse monoclonal anti-FLAG
562 clone M2 (Sigma-Aldrich, 1:200 IFA and 1:500 WB), rabbit monoclonal anti-Flag 8H8L17
563 (ThermoFisher; 1:500 IFA and WB), mouse anti-HRP2 clone 2G12 (1:500 IFA) (95), rabbit
564 polyclonal anti-SBP1 (BR28, 1:500 IFA) (96), mouse monoclonal anti-EXP2 clone 7.7 (1:500 WB)
565 (97), rabbit polyclonal anti-*Plasmodium* Aldolase ab207494 (Abcam; 1:500 WB) and rabbit
566 polyclonal anti-ACP1 (1:500 IFA) (39, 98). Secondary antibodies used were anti-mouse antibody
567 conjugated to Alexa Fluor 488 or 546 and anti-rabbit antibody conjugated to Alexa Fluor 488, (Life
568 Technologies, 1:1000). Parasites were mounted with ProLong diamond with 4',6'-diamidino-2-
569 phenylindole (DAPI) (P36931; Invitrogen) and imaged using a using ZEISS Axio Observer. Image
570 processing, analysis, and display were performed using ZEISS Blue software and Adobe
571 Photoshop. Adjustments to brightness and contrast were made for display purposes.
572
573 **Quantification of protein knockdown.** To evaluate the level of HSP101 protein knockdown,
574 HSP101-kER$^{TetR\text{-}DOZI}$ parasites were synchronized via magnet purification and treated with DMSO
575 or rapamycin before removal of aTc. After aTc removal, parasites were seeded at ~1%
576 parasitemia with different dilutions of aTc and allowed to grow for 48hrs. Using an Attune NxT
577 (ThermoFisher) cytometer, infected RBCs were gated using Hoechst (34580, Invitrogen) and
578 mNG fluorescence was subsequently measured on infected RBCs using the blue laser (488nm)
579 with emission filter (430/30nm). The same procedure was applied for saponin-released parasites
580 after protease treatment as described above.
581
582 **Western blotting.** Western blotting for *Plasmodium* parasites was performed as described
583 previously (38, 55). Briefly, parasites were selectively permeabilized by treatment with ice-cold

584 0.03% saponin in PBS for 15 min followed by lysis with RIPA to remove the hemozoin. For
585 constructs expressed using the *attB* locus, parasites were grown in 500nM aTc for 24hrs prior to
586 incubation with DMSO or Rap to allow expression of the constructs. For the HSP101-kER$^{TetR-DOZI}$
587 lines, parasites were treated with DMSO or rapamycin before removal of aTc. After aTc removal,
588 parasites were seeded at ~1% parasitemia with different dilutions of aTc and allowed to grow for
589 48hrs before purification. The antibodies used in this study were mouse anti-HA antibody (clone
590 16B12; BioLegend, 1:500), mouse anti-FLAG (Clone M2; Sigma-Aldrich, 1:500), and mouse anti-
591 EXP2 (Clone 7.7; 1:500). The secondary antibodies used are IRDye 680CW goat anti-rabbit IgG
592 and IRDye 800CW goat anti-mouse IgG (LICOR Biosciences) (1:20,000). Western blot images
593 were processed using the Odyssey Clx LICOR infrared imaging system software (LICOR
594 Biosciences). Full length blots can be seen in Figures S5,S7.
595

596 **Acknowledgements**

597 This work was supported by NIH grant HL133453 to JRB. The funders had no role in study design,
598 data collection and interpretation, or the decision to submit the work for publication. We thank J.
599 McBride, D. Cavanaugh and EMRR for the EXP2 antibody, C. Braun-Breton for the SBP1
600 antibody and A. Waters for the HP DiCre *P. berghei* parasites.
601

602 **Figures**

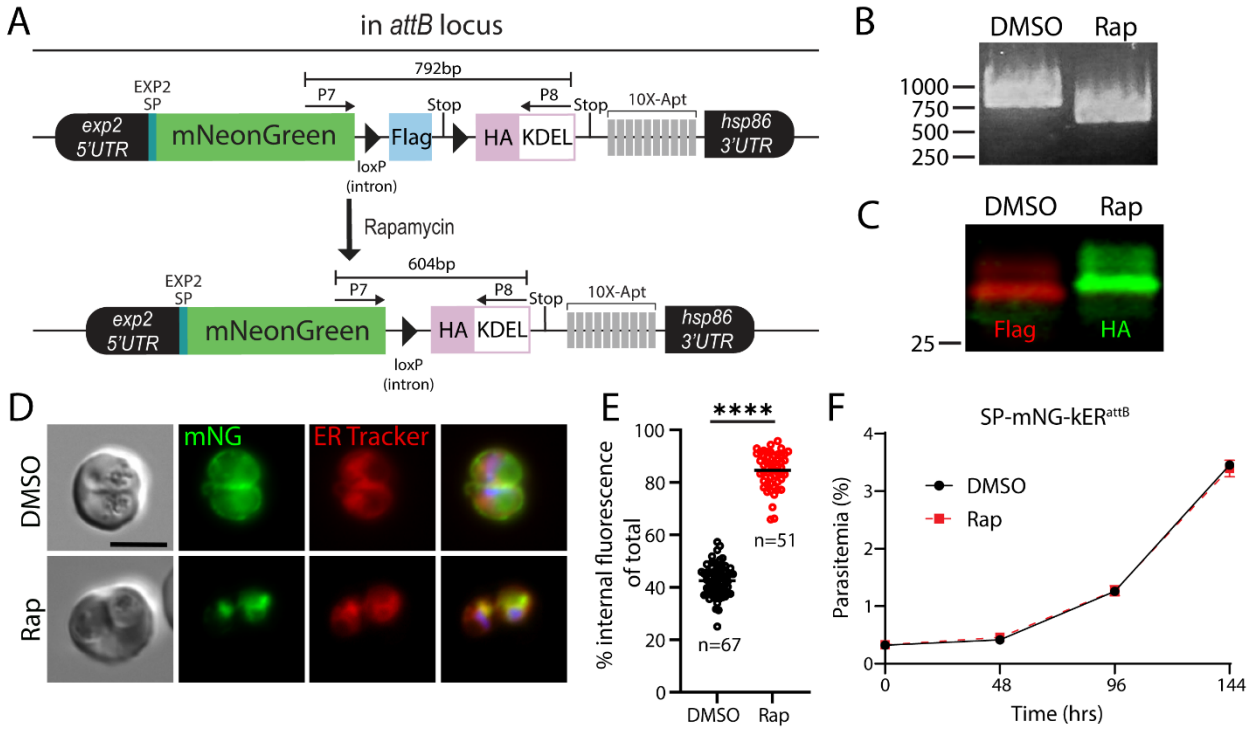

603

604 **Figure 1. Conditional ER retrieval of a secreted reporter does not impact parasite fitness.**
605 A) Schematic of reporter expression cassette installed at the *attB* site of chromosome 6. An
606 mNeonGreen reporter is fused to the signal peptide of EXP2 and expressed under control of the
607 *exp2* promoter. A 3xFLAG tag and stop codon are flanked by loxP-containing introns (triangles)
608 followed by a 3xHA-KDEL, stop codon and 10X aptamer array. Activation of DiCre by rapamycin
609 treatment excises the FLAG tag, bringing into frame the HA-KDEL tag. B) PCR showing excision
610 in mNG-kER parasites 24hrs after rapamycin treatment using primers P7/8. C) Western blot of
611 reporter 24hrs post treatment with DMSO or rapamycin. Molecular weights after signal peptide
612 cleavage are predicted to be 30.8 kDa for mNG-3xFLAG and 30.9 kDa for mNG-3xHA-KDEL. D)
613 Live microscopy of DMSO or rapamycin-treated parasites 24hrs post-treatment. E) Quantification
614 of percent internal mNG fluorescence 168hrs post-treatment with DMSO or rapamycin. Data are
615 pooled from 2 independent experiments and bar indicates mean (****, P<0.0001; unpaired t test).
616 F) Representative growth of asynchronous parasites (n=2 biological replicates) treated with

617 DMSO or rapamycin. Data are presented as means ± standard deviation from one biological
618 replicate (n = 3 technical replicates). All cultures were maintained in media supplemented with
619 500 nM aTc. Scale bar, 5μm.

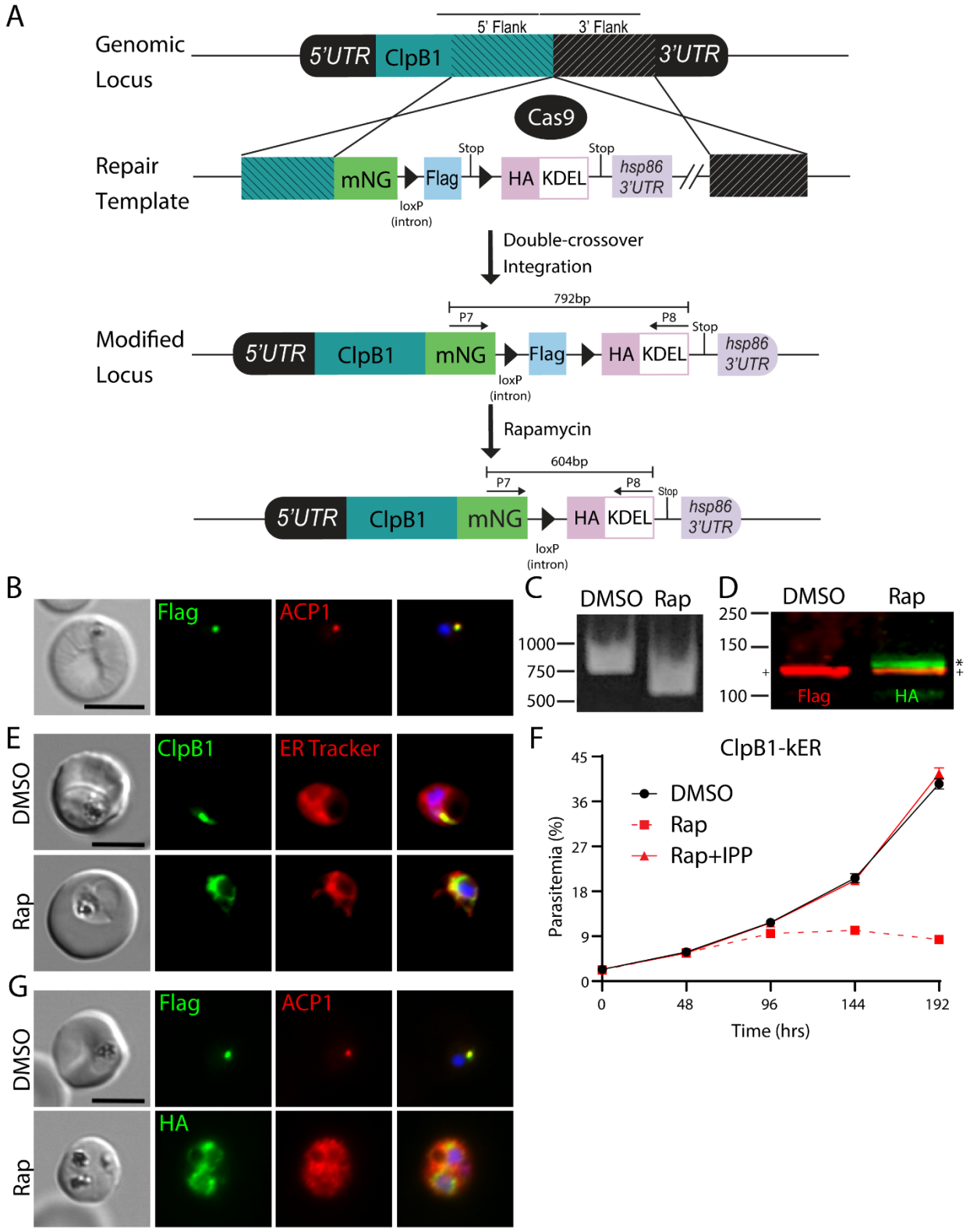

Figure 2. Lethal ER retention of the apicoplast chaperone ClpB1 is rescued by IPP. A) Schematic showing strategy for appending kER to the C-terminus of *clpB1*. B) IFA of PFA fixed

622 parasites stained with mouse anti-Flag and rabbit anti-ACP1 antibodies. C) PCR showing excision
623 in ClpB1-kER parasites 24hrs after rapamycin treatment using primers P7/8. D) Western blot
624 24hrs post treatment with DMSO or rapamycin. Molecular weights after transit peptide cleavage
625 are predicted to be 135 kDa for ClpB1-mNG-3xFLAG and 135.1 kDa for ClpB1-mNG-3xHA-KDEL.
626 (+) represents the mature form of ClpB1 while the (*) represents ClpB1 with the transit peptide
627 still attached. E) Live microscopy of DMSO or rapamycin-treated parasites 48hrs post-treatment.
628 F) Representative growth of asynchronous parasites (n=3 biological replicates) treated with
629 DMSO or rapamycin, with or without supplementation with 200 μM IPP. Data are presented as
630 means ± standard deviation from one biological replicate (n = 3 technical replicates). G) IFA of
631 PFA fixed parasites stained with mouse anti-Flag or anti-HA and rabbit anti-ACP1 antibodies after
632 3 growth cycles where rapamycin treated parasites were supplemented with 200 μM IPP. Scale
633 bars, 5μm.
634

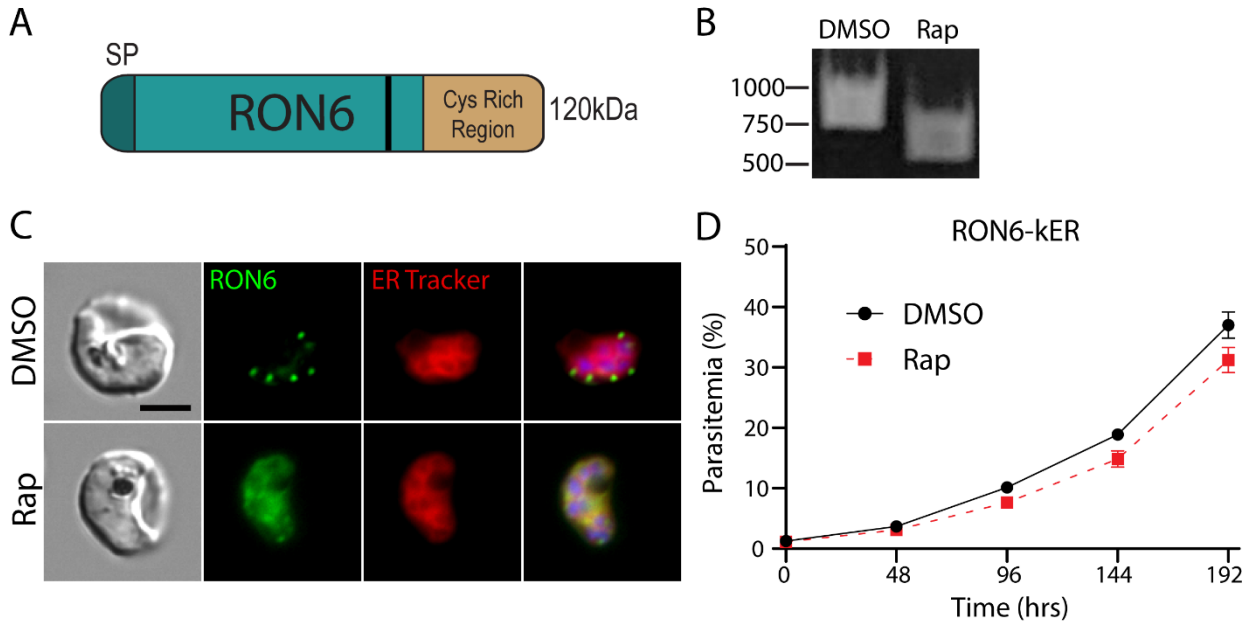

Figure 3. ER retention of rhoptry protein RON6 is tolerated by blood stage parasites. A) Schematic of rhoptry neck protein RON6. SP= signal peptide; black bar= site of piggybac insertion in RON6 (48). B) PCR showing excision in RON6-kER parasites 24hrs after treatment with rapamycin using primers P7/8. C) Live microscopy of DMSO or rapamycin-treated RON6-kER parasites 24hrs post-treatment. D) Representative growth of asynchronous RON6-kER parasites (n=3 biological replicates) treated with DMSO or rapamycin. Data are presented as means ± standard deviation from one biological replicate (n = 3 technical replicates). Scale bar, 5μm.

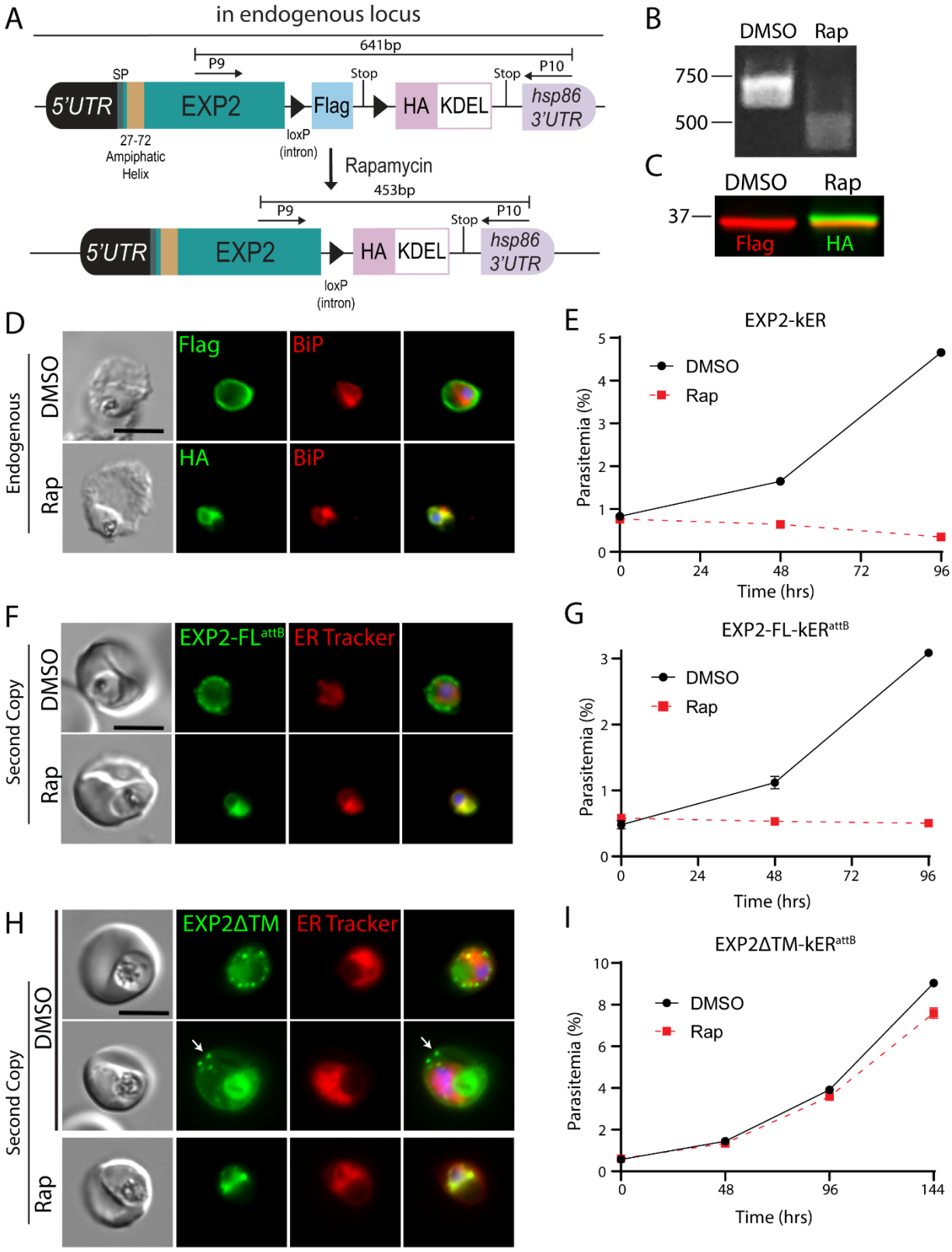

642 **Figure 4. ER retention of EXP2 causes a lethal fitness defect independent of loss of PVM**

643 **transport functions.** A) Schematic showing strategy for appending kER to the endogenous C-

644 terminus of EXP2 without mNG. B) PCR showing excision in EXP2-kER 24hrs after treatment
645 with rapamycin using primers P9/10 C) Western blot of EXP2-kER parasites 24hrs post treatment
646 with DMSO or rapamycin. Molecular weights after signal peptide cleavage are predicted to be
647 34.6 kDa for EXP2-3xFLAG and 34.7 kDa for EXP2-3xHA-KDEL. D) IFA of EXP2-kER 24hrs post-
648 treatment with DMSO or rapamycin. E) Growth of asynchronous parasites (n=2 biological
649 replicates) treated with DMSO or rapamycin. Data are presented as means ± standard deviation
650 from one biological replicate (n = 3 technical replicates). F) Live microscopy of parasites
651 expressing a full-length second copy of EXP2 with an mNG-kER fusion from the *attB* site under
652 the control of the endogenous *exp2* promoter (EXP2-FL-kER^{attB}). Parasites were viewed 24hrs
653 after treatment with DMSO or rapamycin. G) Representative growth of asynchronous EXP2-FL-
654 kER^{attB} parasites (n=2 biological replicates) treated with DMSO or rapamycin. Data are presented
655 as means ± standard deviation from one biological replicate (n = 3 technical replicates). H) Live
656 microscopy of parasites expressing a second copy of EXP2 with mNG-kER fusion and lacking
657 the amphipathic helix from the *attB* site (EXP2ΔTM-kER^{attB}). Parasites were viewed 24hrs after
658 treatment with DMSO or rapamycin. Two representative examples of unexcised parasites are
659 presented, showing localization of the ΔTM version of EXP2 to the PV and host cell in some
660 infected RBCs (arrow). Digestive vacuole fluorescence was also observed as is typical for PV
661 proteins. I) Representative growth of asynchronous EXP2ΔTM-kER^{attB} parasites (n=2 biological
662 replicates) treated with DMSO or rapamycin. Data are presented as means ± standard deviation
663 from one biological replicate (n = 3 technical replicates). Scale bar, 5μm.

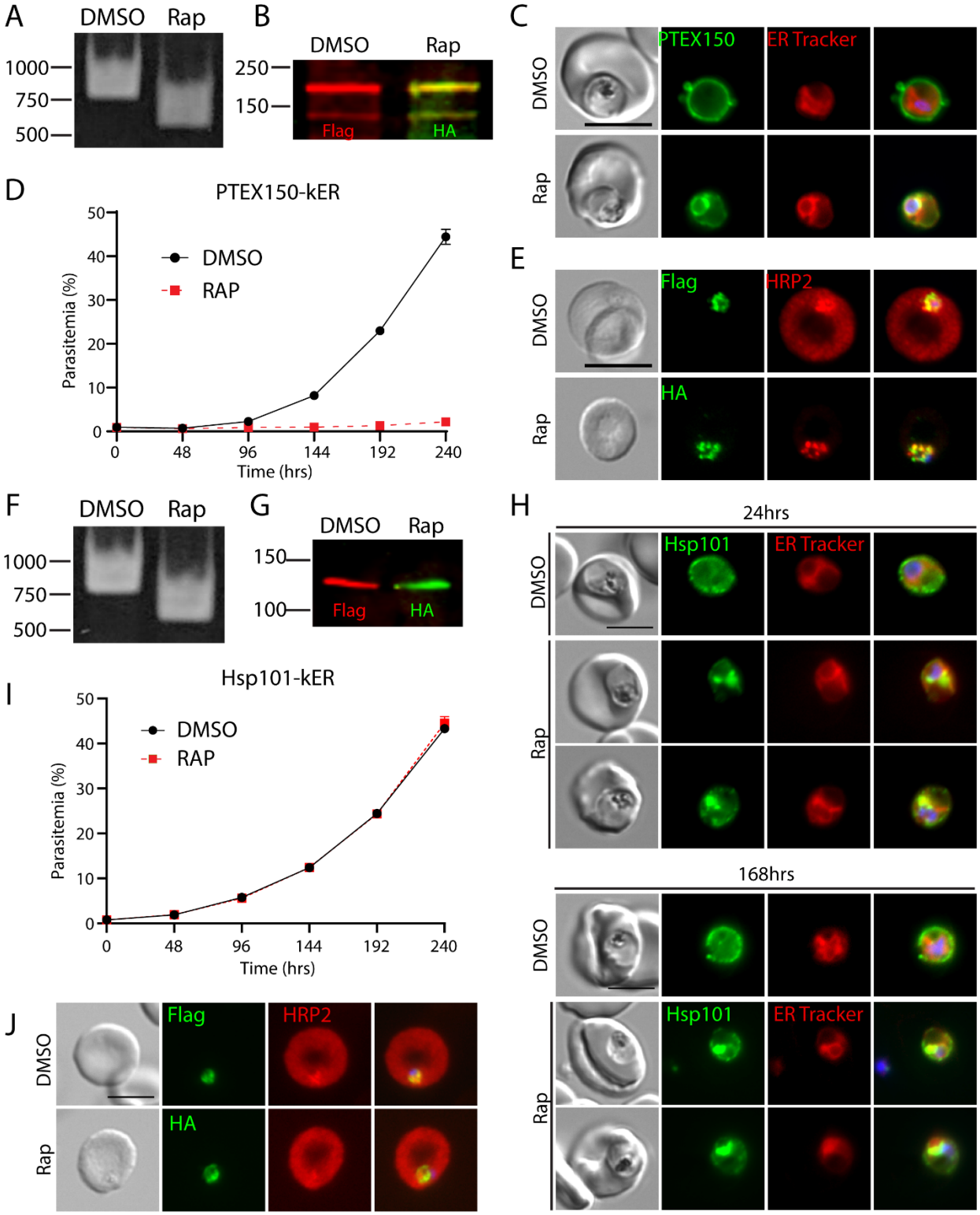

Figure 5. ER retention of PTEX150 but not HSP101 causes a lethal block in protein export. A) PCR showing excision in PTEX150-kER parasites 24hrs after rapamycin treatment using primers P7/8. B) Western blot of PTEX150-kER 24hrs post-treatment with DMSO or rapamycin.

667 Molecular weights after signal peptide cleavage are predicted to be 141 kDa for PTEX150-mNG-
668 3xFLAG and 141.1 kDa for PTEX150-mNG-3xHA-KDEL. Note that PTEX150 is observed to
669 migrate at higher molecular weight than predicted (61). C) Live microscopy of PTEX150-kER
670 24hrs post-treatment with DMSO or rapamycin-treated. D) Representative growth of
671 asynchronous PTEX150-kER parasites (n=3 biological replicates) treated with DMSO or
672 rapamycin. Data are presented as means ± standard deviation from one biological replicate (n = 3
673 technical replicates). E) IFA of synchronized, ring-stage PTEX150-kER parasites 48hrs post-
674 treatment with DMSO or rapamycin and probed with anti-HRP2 and anti-FLAG or anti-HA
675 antibodies. F) PCR showing excision in HSP101-kER parasites 24hrs after rapamycin treatment
676 using primers P7/8. G) Western blot of HSP101-kER parasites 14 days post-treatment with DMSO
677 or rapamycin. Molecular weights after signal peptide cleavage are predicted to be 130.5 kDa for
678 HSP101-mNG-3xFLAG and 130.6 kDa for HSP101-mNG-3xHA-KDEL. H) Live microscopy of
679 HSP101-kER 24hrs and 168hrs post-treatment with DMSO or rapamycin. I) Representative
680 growth of asynchronous HSP101-kER parasites (n=3 biological replicates) treated with DMSO or
681 rapamycin. Data are presented as means ± standard deviation from one biological replicate (n = 3
682 technical replicates). J) IFA of synchronized, ring-stage HSP101-kER parasites 48hrs post-
683 treatment with DMSO or rapamycin and probed with anti-HRP2 and anti-FLAG or anti-HA
684 antibodies. Scale bar, 5μm.

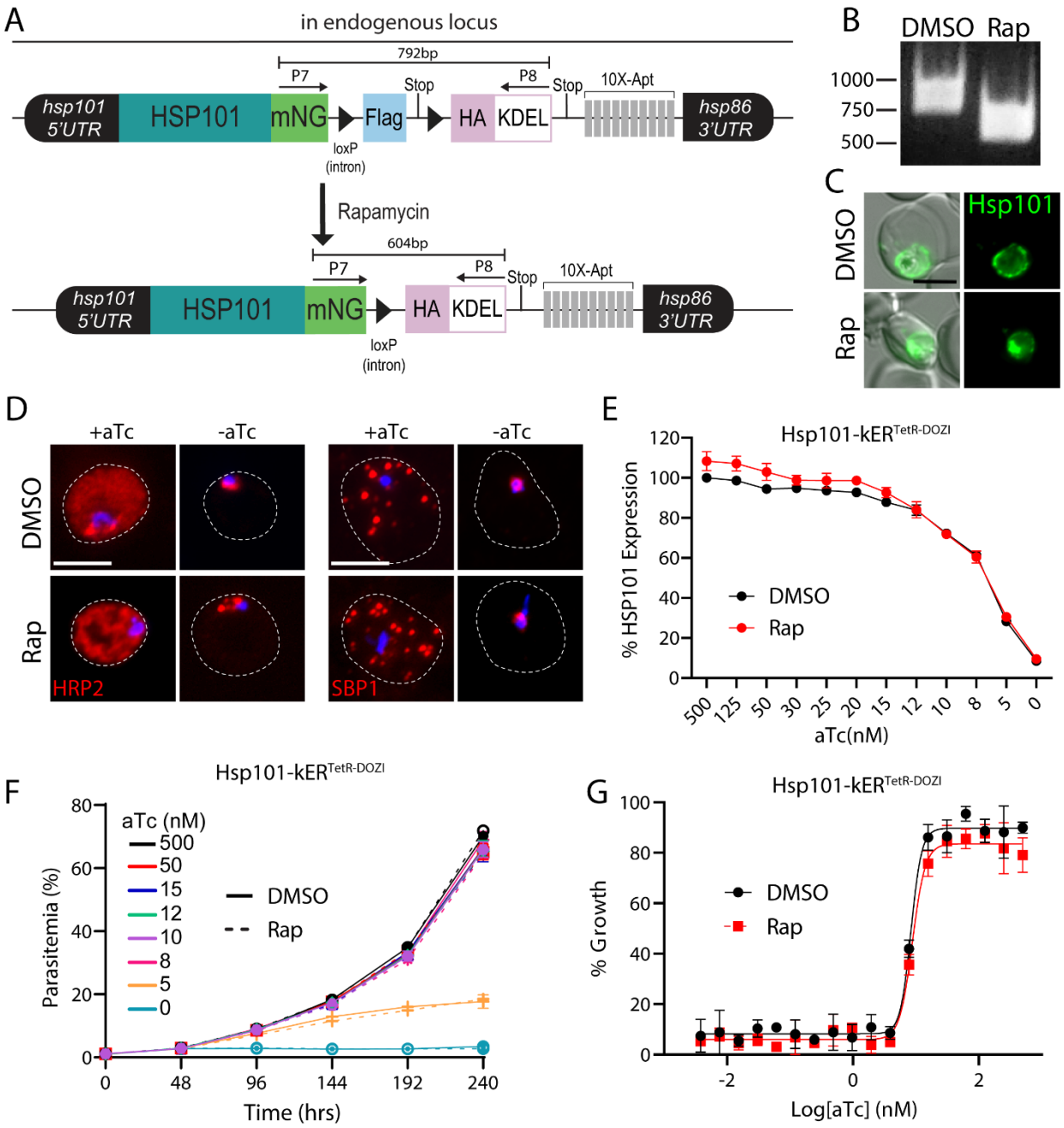

Figure 6. Depletion of HSP101 PV levels does not hypersensitize parasites to HSP101 knockdown. A) Schematic showing strategy for appending kER and the TetR-DOZI aptamers system to the endogenous C-terminus of HSP101. B) PCR showing excision in HSP101-kER$^{TetR-DOZI}$ parasites 24hrs after rapamycin treatment using primers P7/8. C) Live microscopy of HSP101-kER$^{TetR-DOZI}$ parasites 168hrs post-treatment with DMSO or rapamycin. D) IFA detecting the soluble PEXEL protein HRP2 or the transmembrane PNEP SBP1 in synchronized, ring-stage

691 HSP101-kER$^{TetR-DOZI}$ parasites grown for 48hrs +/- aTc and treated with DMSO or rapamycin 1
692 cycle prior. E) Quantification of HSP101 levels by flow cytometry measurement of mNeonGreen
693 fluorescence in HSP101-kER$^{TetR-DOZI}$ parasites grown for 48 hrs at indicated aTc concentrations
694 and treated with DMSO or rapamycin 2 cycles prior. MFI data were normalized to DMSO-treated
695 parasites grown in 500 nM aTc (100%) and presented as mean ± SEM (n = 5 biological replicates).
696 F) Representative growth curves (n = 4 biological replicates) of HSP101-kER$^{TetR-DOZI}$ parasites
697 grown at indicated aTc concentrations and treated with DMSO or rapamycin 2 cycles prior. Data
698 are presented as means ± standard deviation from one biological replicate (n = 3 technical
699 replicates). G) Representative EC_{50} shift assay (n=3 biological replicates) of parasites treated with
700 DMSO or rapamycin with two-fold dilutions of aTc starting at 500nM. Data are presented as
701 means ± standard deviation from one biological replicate (n = 3 technical replicates). Scale bars,
702 5μm.
703

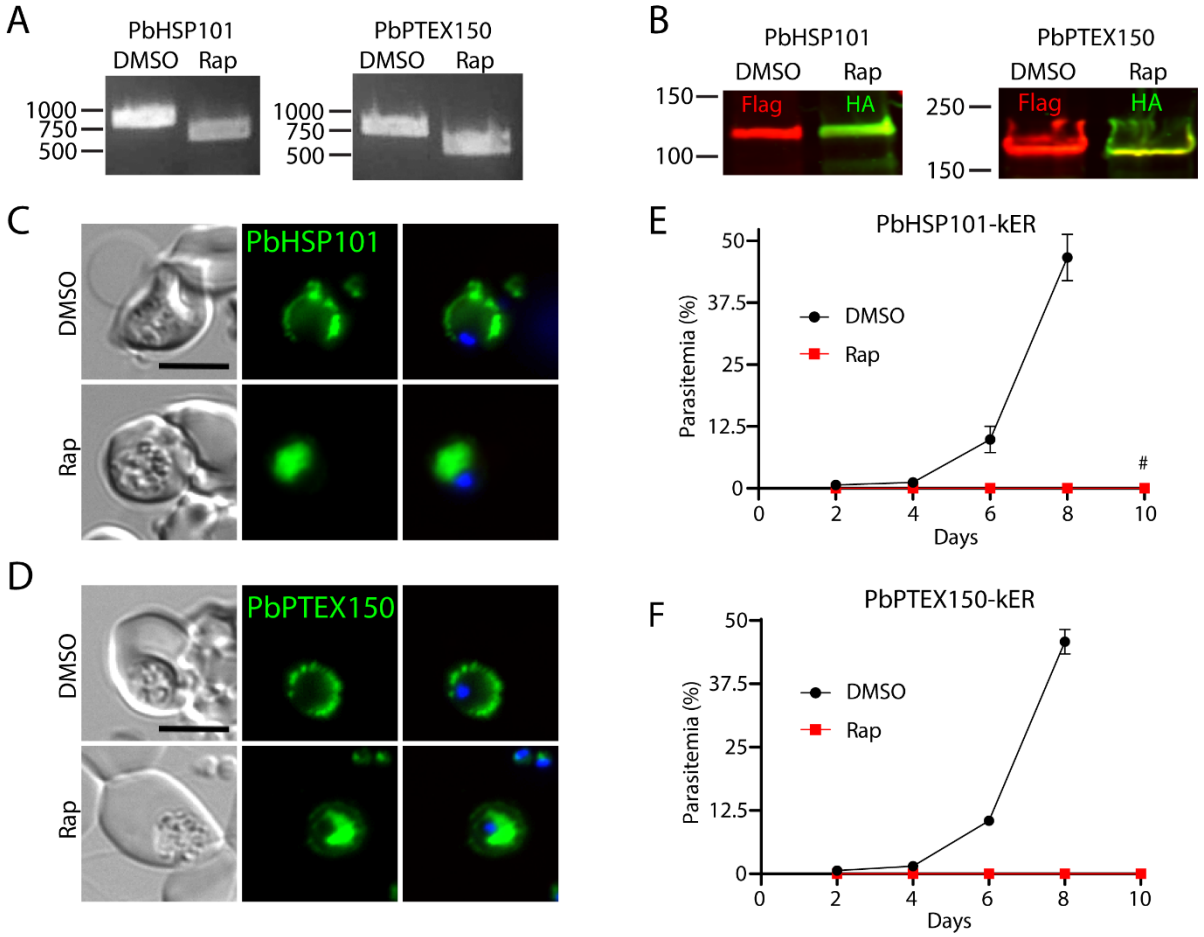

Figure 7: ER retention of HSP101 is lethal *in vivo*. A) PCR showing excision in PbPTEX150-kER and PbHSP101-kER *P. berghei* parasites treated with rapamycin and cultured 18hrs *ex vivo* using primers P7/P60. B) Western blot of PbPTEX150-kER and PbHSP101-kER parasites 24hrs post-treatment with DMSO or rapamycin. Molecular weights after signal peptide cleavage are predicted to be 130.9 kDa for PbHSP101-mNG-3xFLAG, 131 kDa for PbHSP101-mNG-3xHA-KDEL, 130.5 kDa for PbPTEX150-mNG-3xFLAG and 130.6 kDa for PbPTEX150-mNG-3xHA-KDEL. Note that PbPTEX150 is observed to migrate at higher molecular weight than predicted (99). C,D) Live microscopy of PbHSP101-kER or PbPTEX150-kER parasites 18hrs post-treatment with DMSO or rapamycin. E,F) Parasitemia of PbHSP101-kER or PbPTEX150-kER infected mice inoculated by tail vein-injection of parasites treated *ex vivo* with DMSO or rapamycin. Data are presented as means ± standard deviation of three independent experiments (one mouse infected per treatment in each experiment). No parasites were observed in mice

716 injected with rapamycin treated parasites except that one mouse injected with rapamycin-treated
717 PbHSP101-kER parasites became patent on day 10 (#). However, PCR showed these parasites
718 had not undergone excision (see Figure S6C). Scale bar, 5μm.

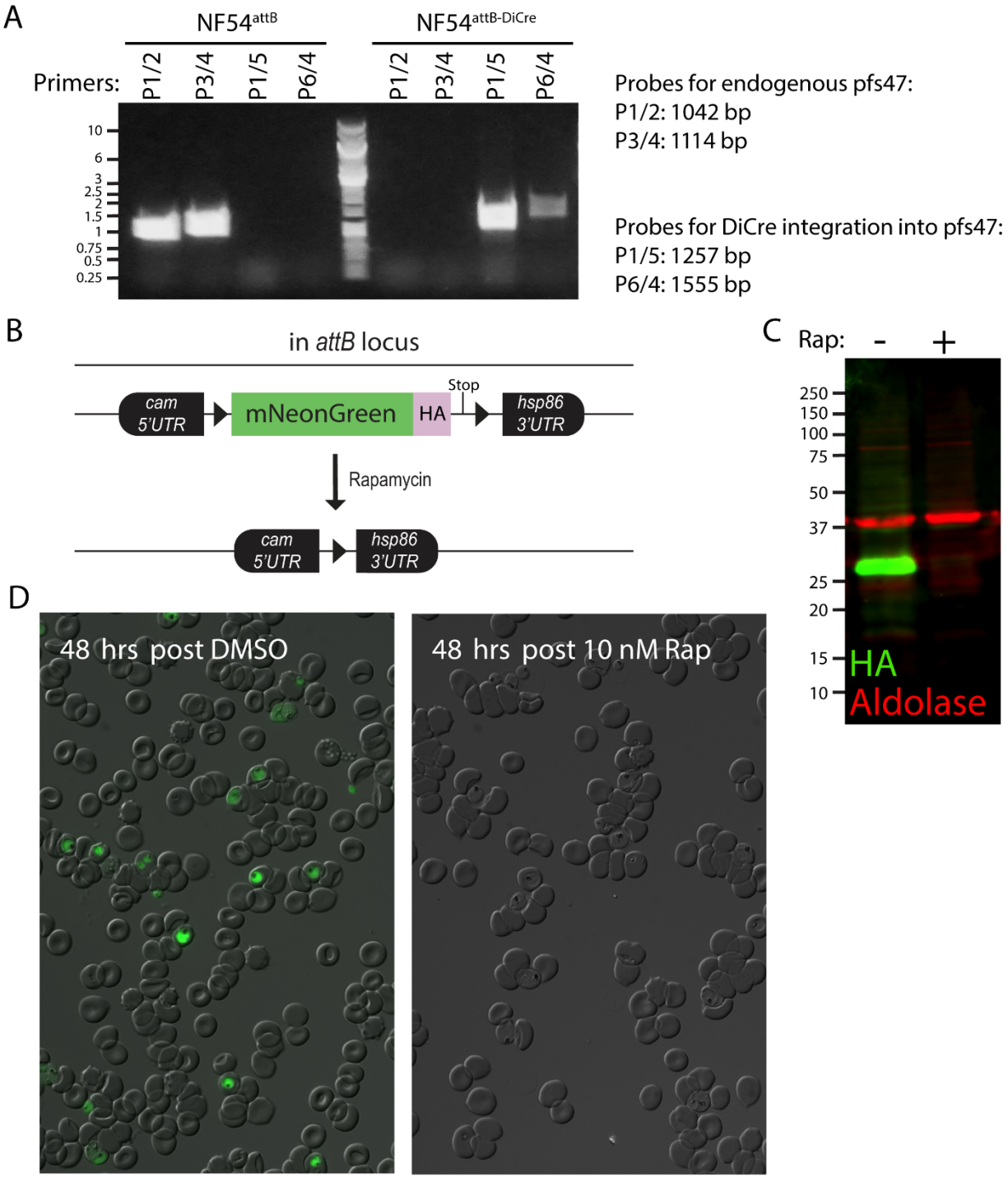

Figure S1. Generation and validation of NF54$^{attB\text{-}DiCre}$ parasites. A) Diagnostic PCR showing DiCre cassette integration into the *pfs47* locus using primers P1/2 and P3/4 to detect unmodified locus, and primers P1/5 and P6/4 to detect integration. B) Schematic of reporter integrated at *attB* in *cg6* to test DiCre functionality in NF54$^{attB\text{-}DiCre}$. C) Western blot and D) live microscopy of

723 parasites 48hrs after 3hr treatment with DMSO or 10nM rapamycin. Molecular weights are
724 predicted to be 30 kDa for mNG-3xHA and 40.1 kDa for aldolase.
725

726

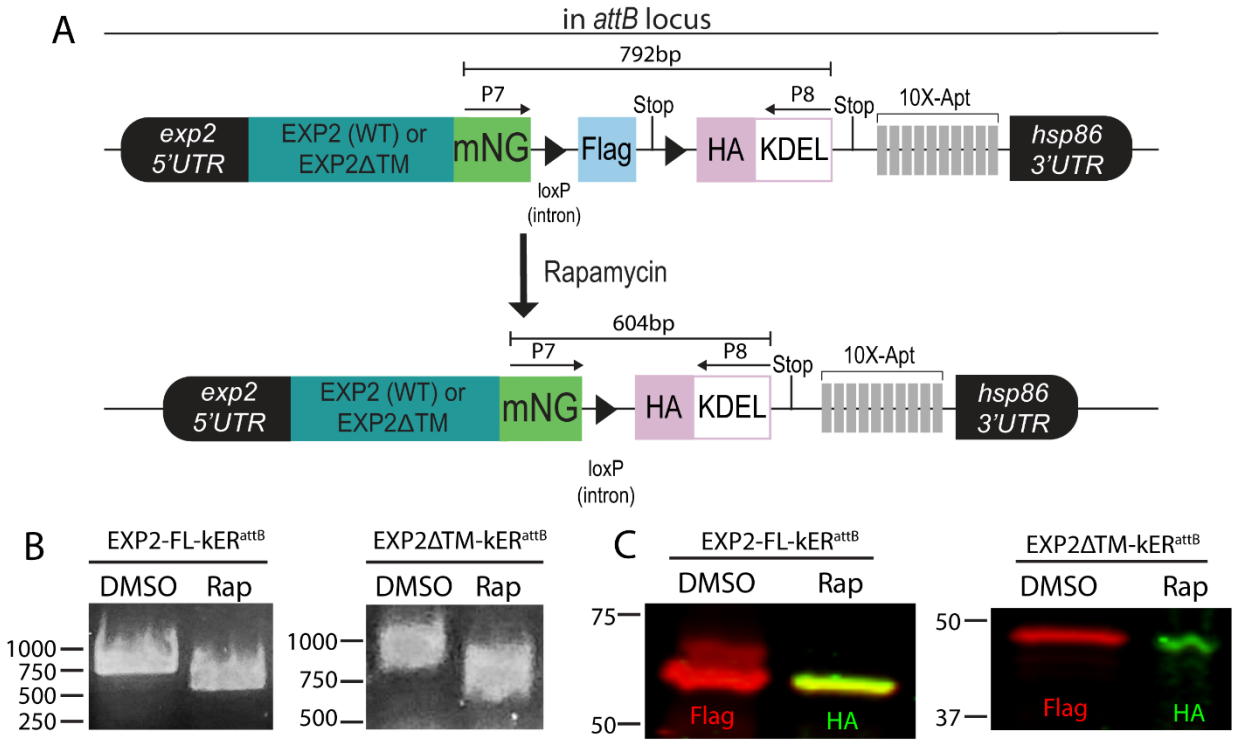

727 **Figure S2. Validation of DiCre-mediated excision in second copy EXP2-kER parasites.** A)
728 Schematic showing cassette for second copy expression of full-length EXP2 or a version lacking
729 the amphipathic helix with kER fusion from the *attB* site of chromosome 6. B) PCR showing
730 excision in EXP2-FL-kER^{attB} and EXP2ΔTM-kER^{attB} parasites 24hrs after rapamycin treatment
731 using primers P7/8. C) Western blots from second copy EXP2-kER parasite samples taken 24hrs
732 after DMSO or rapamycin treatment showing conversion from Flag to HA.

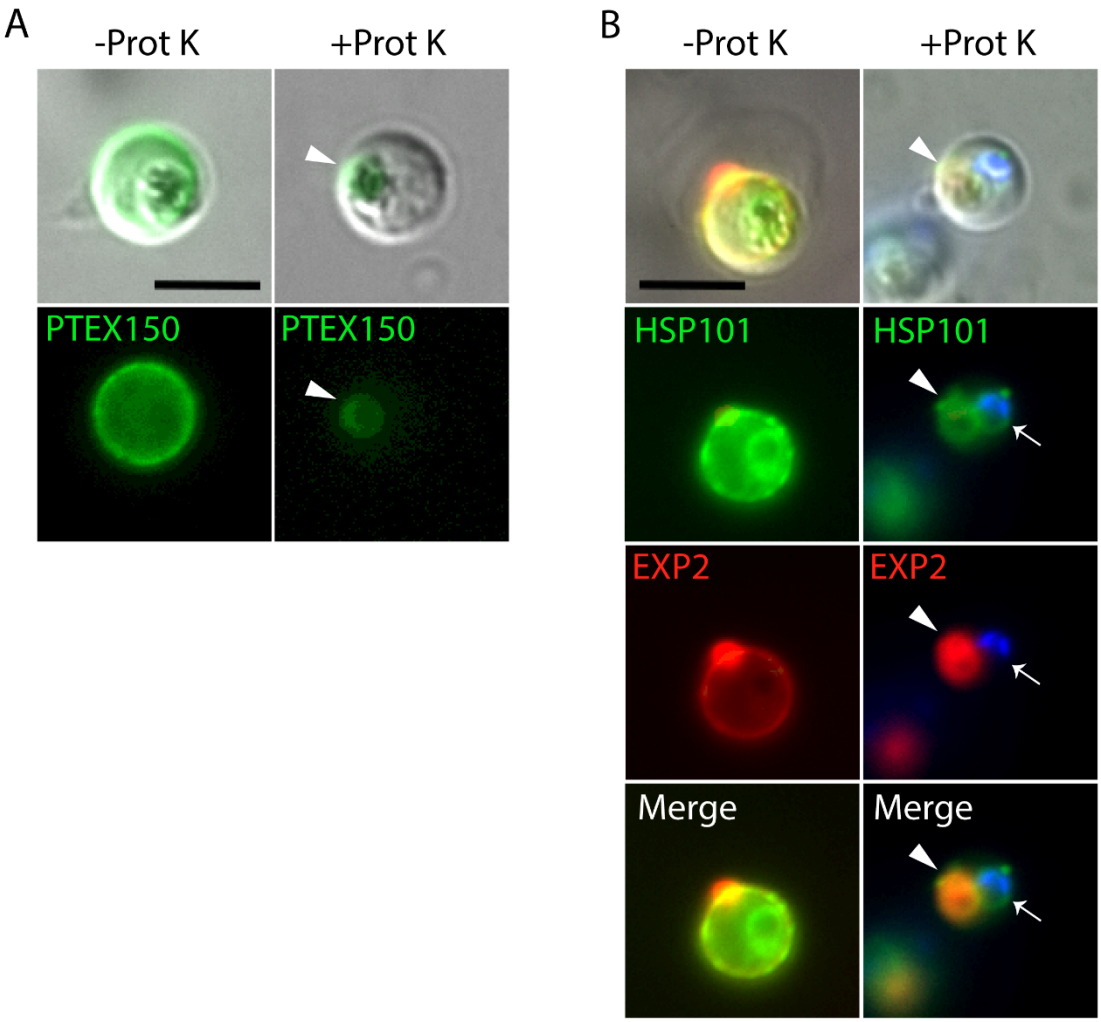

733 **Figure S3. Protease protection assay on live cells verifies an internal, perinuclear pool of**
734 **HSP101 but not EXP2 or PTEX150.** Live microscopy of parasite lines with endogenous
735 fluorescent protein fusions A) PTEX150-mNG-3xFLAG or B) EXP2-mRuby3 and HSP101-mNG
736 treated with saponin +/- Proteinase K. Images are representative of n=2 biological replicates.
737 Arrowhead: protease-protected fluorescence within the digestive vacuole from endocytosis
738 typically seen for PV proteins; arrow: protease-protected perinuclear fluorescence unique to
739 HSP101. Scale bar, 5μm.
740

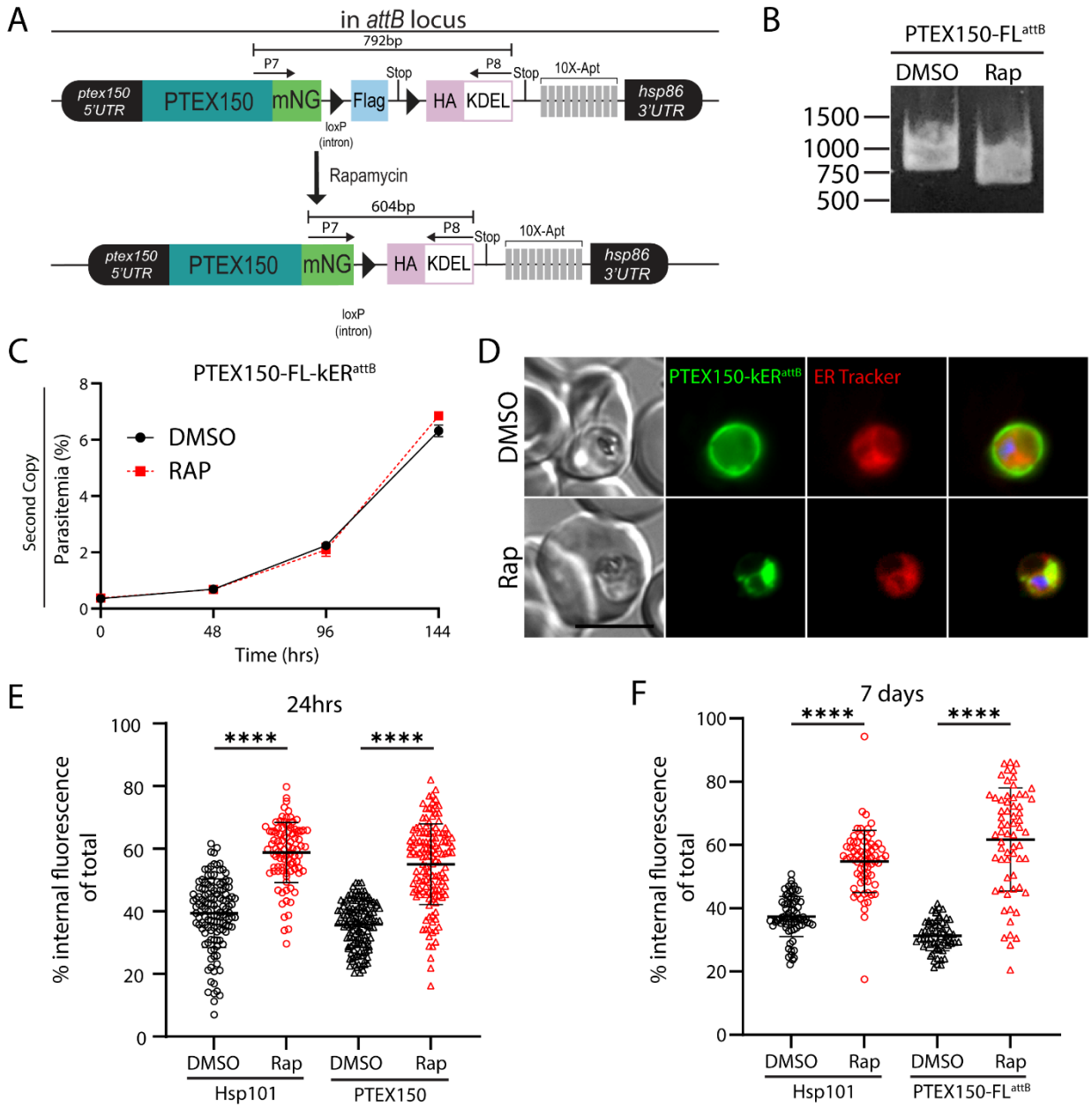

Figure S4. Supporting data for Figure 5. A) Schematic showing cassette for second copy expression of PTEX150-kER from the *attB* site of chromosome 6. B) PCR showing excision in PTEX150-kER^{attB} parasites 24hrs after rapamycin treatment using primers P7/8. C) Representative growth curves of asynchronous, second copy PTEX150-kER parasites (n=3 biological replicates) treated with DMSO or rapamycin. Data are presented as means ± standard deviation from one biological replicate (n = 3 technical replicates). D) Live microscopy of second copy PTEX150-kER parasites 24hrs post-treatment with DMSO or rapamycin. E) Quantification

748 of percent internal mNG fluorescence in live microcopy images of endogenously tagged HSP101-
749 and PTEX150-kER parasites 24hrs post-treatment with DMSO or rapamycin. Data are pooled
750 from 3 (HSP101) or 2 (PTEX150) independent experiments and bars indicate mean ± standard
751 deviation (****, P<0.0001; unpaired t test). F) Quantification of percent internal mNG fluorescence
752 in live microcopy images of endogenously tagged HSP101-kER and second copy PTEX150-kER
753 parasites lines 168hrs post-treatment with DMSO or rapamycin. Data are pooled from 2
754 independent experiments and bars indicate represented as means ± standard deviation (****,
755 P<0.0001; unpaired t test).
756

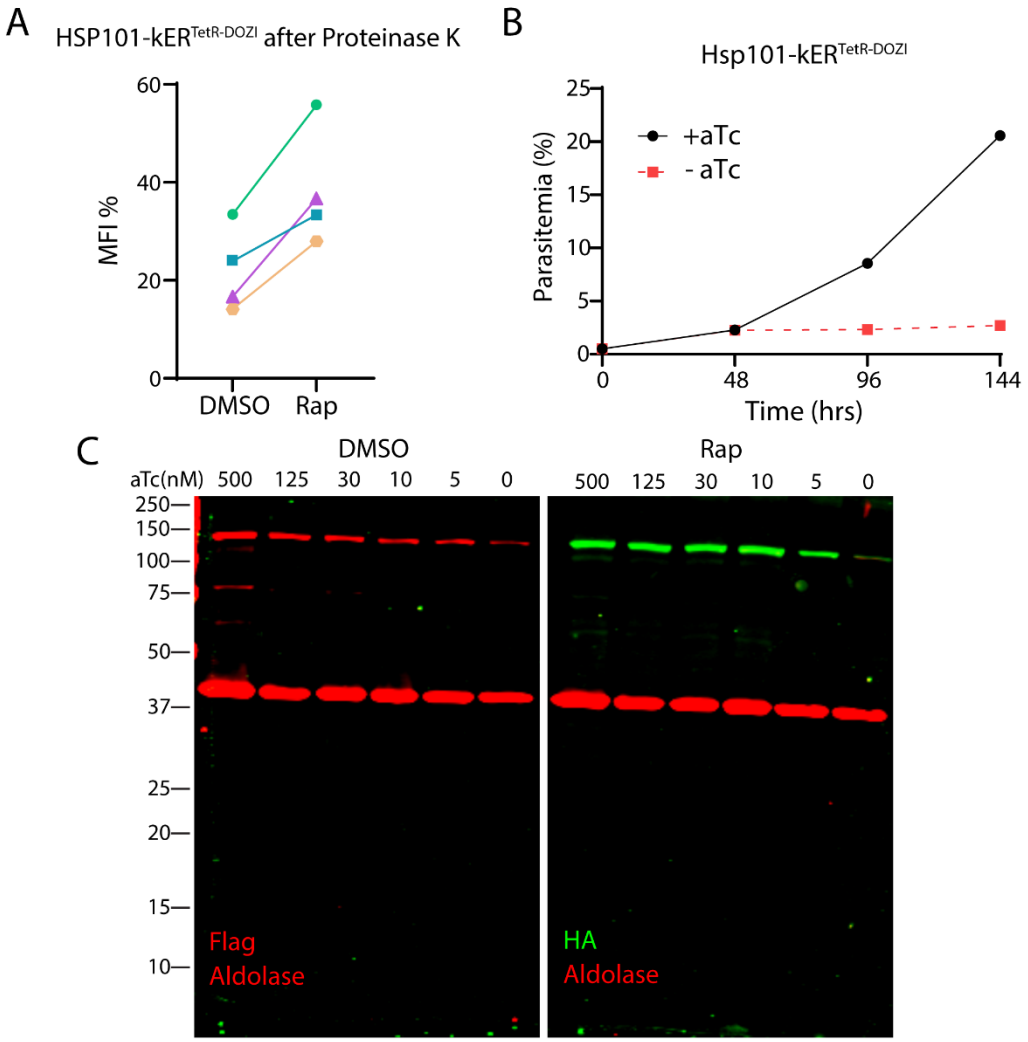

Figure S5. Supporting data for Figure 6. A) Mean fluorescence intensity quantification from proteinase K treated parasites. The amount of protected fluorescent signal (percent of total before protease treatment) was determined by dividing MFI after proteinase K treatment from before proteinase K treatment. Colors represent different replicates. B) Representative growth curve (n = 3 biological replicates) of HSP101-kER$^{TetR\text{-}DOZI}$ parasites grown with or without aTc. Data are presented as means ± standard deviation of one biological replicate (n = 3 technical replicates). C) Western blot of HSP101-kER$^{TetR\text{-}DOZI}$ parasites grown 48hrs at indicated aTc concentrations. Parasites grown in 500 nM aTc were treated with DMSO or rapamycin 24hrs before aTc was washed out and restored at indicated concentrations. Results are representative of 4 independent experiments.

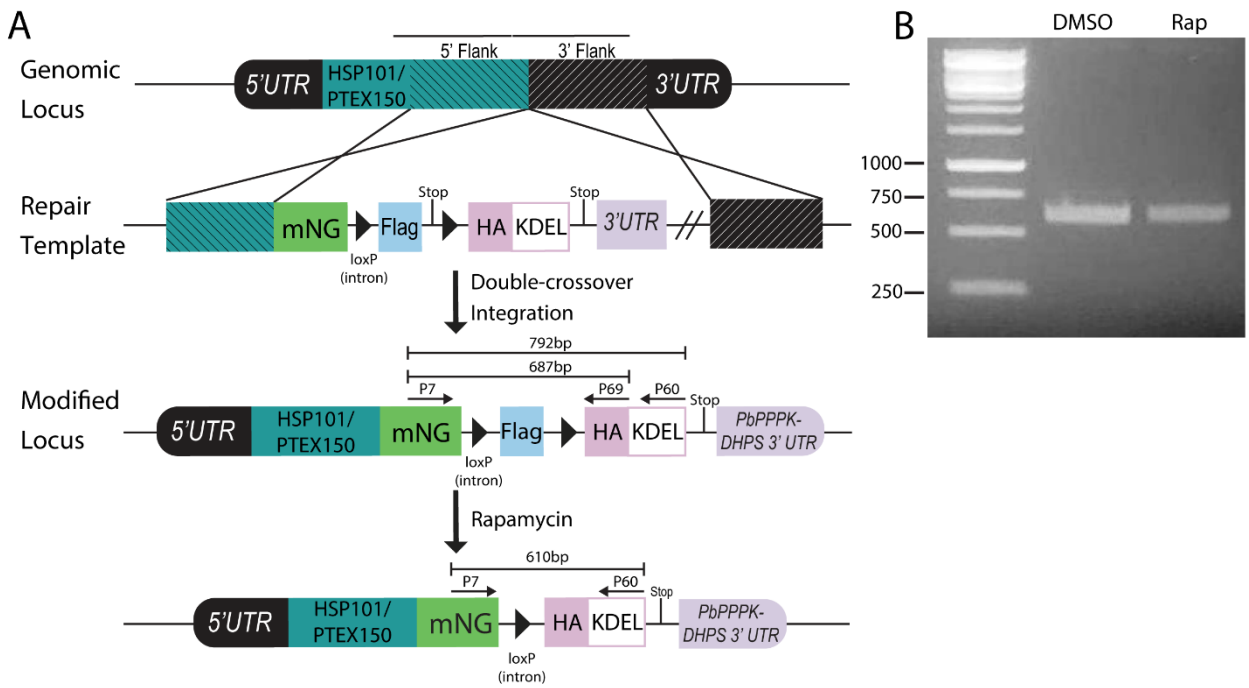

767 **Figure S6. Supporting data for Figure 7.** A) Schematic showing strategy for appending kER to
768 the endogenous C-terminus of *P. berghei hsp101* and *ptex150*. B) PCR using P7/P69 to evaluate
769 excision of the kER cassette in parasites taken from mice injected with DMSO (parasite collected
770 on day 8) or rapamycin-treated PbHSP101-kER (taken from the single mouse where parasites
771 appeared on day 10). The results indicate that the kER cassette was unexcised in the parasites
772 observed in the mouse that became patent on day 10.

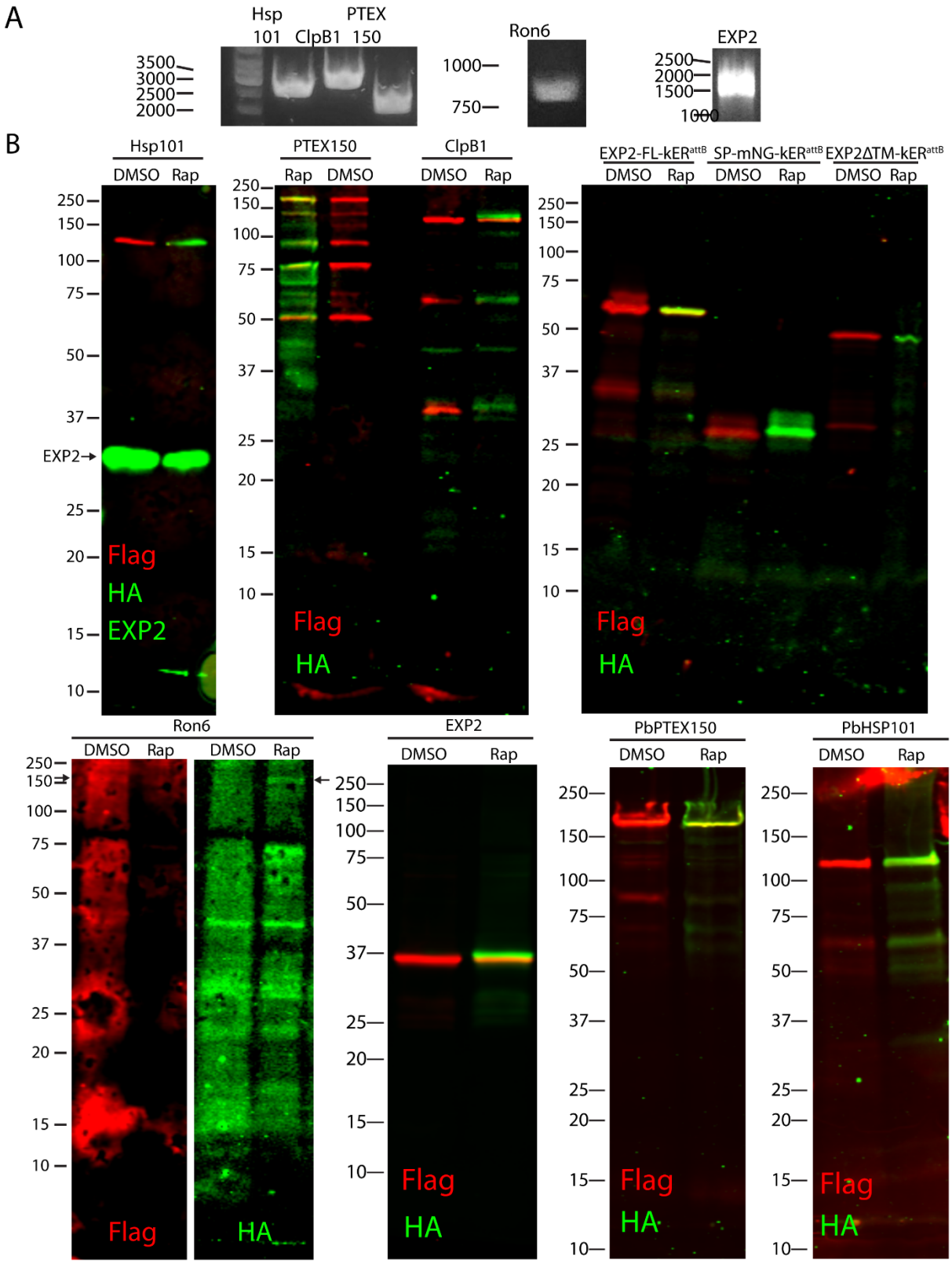

773 **Figure S7. Integration PCRs and Uncropped Western blots** A) Integration PCR for

774 endogenous kER tags using primers P11/P12 (HSP101), P13/P12 (ClpB1), P14/P12 (PTEX150),

775 P15/P16 (RON6), and P17/P8 (EXP2). B) Uncropped Western blots. For RON6-kER, molecular
776 weights after signal peptide cleavage are predicted to be 141.3 kDa for RON6-mNG-3xFLAG and
777 141.4 kDa for RON6-mNG-3xHA-KDEL. Arrows indicate RON6 signal; notice the low expression
778 of RON6, consistent with low expression levels in the blood stage (PlasmoDB). For EXP2-FL-
779 kER^{attB}, molecular weights after signal peptide cleavage are predicted to be 61.1 kDa for EXP2-
780 mNG-3xFLAG and 61.2 kDa for EXP2-mNG-3xHA-KDEL. For EXP2ΔTM-kER^{attB}, molecular
781 weights after signal peptide cleavage are predicted to be 54.2 kDa for EXP2ΔTM-mNG-3xFLAG
782 and 54.3 kDa for EXP2ΔTM-3xHA-KDEL.
783

784 **References**

785 1. O. A. Akuh, R. Elahi, S. T. Prigge, F. Seeber, The ferredoxin redox system - an essential
786 electron distributing hub in the apicoplast of Apicomplexa. *Trends Parasitol* **38**, 868-881
787 (2022).

788 2. M. M. Cova, M. H. Lamarque, M. Lebrun, How Apicomplexa Parasites Secrete and Build
789 Their Invasion Machinery. *Annual Review of Microbiology* **76**, 619-640 (2022).

790 3. J. M. Matz, J. R. Beck, M. J. Blackman, The parasitophorous vacuole of the blood-stage
791 malaria parasite. *Nat Rev Microbiol* 10.1038/s41579-019-0321-3 (2020).

792 4. M. Garten, J. R. Beck, Structured to conquer: transport across the Plasmodium
793 parasitophorous vacuole. *Current Opinion in Microbiology* **63**, 181-188 (2021).

794 5. T. F. De Koning-Ward, M. W. A. Dixon, L. Tilley, P. R. Gilson, Plasmodium species:
795 master renovators of their host cells. *Nature Reviews Microbiology* **14**, 494-507 (2016).

796 6. J. R. Beck, C.-M. Ho, Transport mechanisms at the malaria parasite-host cell interface.
797 *PLOS Pathogens* **17**, e1009394 (2021).

798 7. T. J. Sargeant *et al.*, Lineage-specific expansion of proteins exported to erythrocytes in
799 malaria parasites. *Genome Biol* **7**, R12 (2006).

800 8. J. A. Boddey *et al.*, Role of Plasmepsin V in Export of Diverse Protein Families from the
801 Plasmodium falciparum Exportome. *Traffic* **14**, 532-550 (2013).

802 9. C. Van Ooij *et al.*, The Malaria Secretome: From Algorithms to Essential Function in
803 Blood Stage Infection. *PLoS Pathogens* **4**, e1000084 (2008).

804 10. J. Schulze *et al.*, The Plasmodium falciparum exportome contains non-canonical
805 PEXEL/HT proteins. *Mol Microbiol* **97**, 301-314 (2015).

806 11. T. K. Jonsdottir, M. Gabriela, B. S. Crabb, F. d. K.-W. T, P. R. Gilson, Defining the
807 Essential Exportome of the Malaria Parasite. *Trends Parasitol* **37**, 664-675 (2021).

808 12. S. Tomavo, C. Slomianny, M. Meissner, V. B. Carruthers, Protein trafficking through the
809 endosomal system prepares intracellular parasites for a home invasion. *PLoS*
810 *Pathogens* **9**, e1003629 (2013).

811 13. A. Florentin, D. W. Cobb, H. M. Kudyba, V. Muralidharan, Directing Traffic: Chaperone-
812 mediated protein transport in malaria parasites. *Cell Microbiol* 10.1111/cmi.13215,
813 e13215 (2020).

814 14. P. Brauer *et al.*, Structural basis for pH-dependent retrieval of ER proteins from the Golgi
815 by the KDEL receptor. *Science* **363**, 1103-1107 (2019).

816 15. S. Munro, H. R. B. Pelham, A C-terminal signal prevents secretion of luminal ER
817 proteins. *Cell* **48**, 899-907 (1987).

818 16. A. Gerondopoulos *et al.*, A signal capture and proofreading mechanism for the KDEL-
819 receptor explains selectivity and dynamic range in ER retrieval. *eLife* **10** (2021).

820 17. H. G. Elmendorf, K. Haldar, Identification and localization of ERD2 in the malaria
821 parasite Plasmodium falciparum: separation from sites of sphingomyelin synthesis and
822 implications for organization of the Golgi. *The EMBO Journal* **12**, 4763-4773 (1993).

823 18. N. La Greca, A. R. Hibbs, C. Riffkin, M. Foley, L. Tilley, Identification of an endoplasmic
824 reticulum-resident calcium-binding protein with multiple EF-hand motifs in asexual
825 stages of Plasmodium falciparum. *Mol Biochem Parasitol* **89**, 283-293 (1997).

826 19. H. M. Kudyba *et al.*, The endoplasmic reticulum chaperone PfGRP170 is essential for
827 asexual development and is linked to stress response in malaria parasites. *Cell Microbiol*
828 **21**, e13042 (2019).

829 20. D. W. Cobb *et al.*, A redox-active crosslinker reveals an essential and inhibitable
830 oxidative folding network in the endoplasmic reticulum of malaria parasites. *PLOS*
831 *Pathogens* **17**, e1009293 (2021).

832 21. S. Külzer, N. Gehde, J. M. Przyborski, Return to sender: use of Plasmodium ER retrieval
833 sequences to study protein transport in the infected erythrocyte and predict putative ER
834 protein families. *Parasitology Research* **104**, 1535-1541 (2009).

835 22. M. A. Fierro *et al.*, An ER CREC family protein regulates the egress proteolytic cascade
836 in malaria parasites. *bioRxiv* 10.1101/457481, 457481 (2019).

837 23. M. Gabriela *et al.*, A revised mechanism for how Plasmodium falciparum recruits and
838 exports proteins into its erythrocytic host cell. *PLOS Pathogens* **18**, e1009977 (2022).

839 24. J. R. Beck, V. Muralidharan, A. Oksman, D. E. Goldberg, PTEX component HSP101
840 mediates export of diverse malaria effectors into host erythrocytes. *Nature* **511**, 592-595
841 (2014).

842 25. B. Elsworth *et al.*, PTEX is an essential nexus for protein export in malaria parasites.
843 *Nature* **511**, 587-591 (2014).

844 26. C. M. Ho *et al.*, Malaria parasite translocon structure and mechanism of effector export.
845 *Nature* **561**, 70-75 (2018).

846 27. E. Knuepfer, M. Napiorkowska, C. Van Ooij, A. A. Holder, Generating conditional gene
847 knockouts in Plasmodium – a toolkit to produce stable DiCre recombinase-expressing
848 parasite lines using CRISPR/Cas9. *Scientific Reports* **7** (2017).

849 28. C. R. Collins *et al.*, Robust inducible Cre recombinase activity in the human malaria
850 parasite P lasmodium falciparum enables efficient gene deletion within a single asexual
851 erythrocytic g. *Molecular Microbiology* **88**, 687-701 (2013).

852 29. S. Chaubey, M. Grover, U. Tatu, Endoplasmic Reticulum Stress Triggers
853 Gametocytogenesis in the Malaria Parasite. *Journal of Biological Chemistry* **289**, 16662-
854 16674 (2014).

855 30. A. J. Polino, A. S. Nasamu, J. C. Niles, D. E. Goldberg, Assessment of Biological Role
856 and Insight into Druggability of the Plasmodium falciparum Protease Plasmepsin V. *ACS*
857 *Infect Dis* **6**, 738-746 (2020).

858 31. J. M. Przyborski *et al.*, Trafficking of STEVOR to the Maurer's clefts in Plasmodium
859 falciparum-infected erythrocytes. *The EMBO Journal* **24**, 2306-2317 (2005).

860 32. G. G. Van Dooren *et al.*, Development of the endoplasmic reticulum, mitochondrion and
861 apicoplast during the asexual life cycle ofPlasmodium falciparum. *Molecular*
862 *Microbiology* **57**, 405-419 (2005).

863 33. C. J. Tonkin, N. S. Struck, K. A. Mullin, L. M. Stimmler, G. I. McFadden, Evidence for
864 Golgi-independent transport from the early secretory pathway to the plastid in malaria
865 parasites. *Molecular Microbiology* **61**, 614-630 (2006).

866 34. M. C. S. Lee, P. A. Moura, E. A. Miller, D. A. Fidock, Plasmodium falciparumSec24
867 marks transitional ER that exports a model cargo via a diacidic motif. *Molecular*
868 *Microbiology* **68**, 1535-1546 (2008).

869 35. S. R. Heiny, S. Pautz, M. Recker, J. M. Przyborski, Protein Traffic to thePlasmodium
870 falciparumApicoplast: Evidence for a Sorting Branch Point at the Golgi. *Traffic* **15**, 1290-
871 1304 (2014).

872 36. M. J. Boucher *et al.*, Integrative proteomics and bioinformatic prediction enable a high-
873 confidence apicoplast proteome in malaria parasites. *PLoS Biol* **16**, e2005895 (2018).

874 37. J. Birnbaum *et al.*, A Kelch13-defined endocytosis pathway mediates artemisinin
875 resistance in malaria parasites. *Science* **367**, 51-59 (2020).

876 38. T. Nessel *et al.*, EXP1 is required for organisation of EXP2 in the intraerythrocytic
877 malaria parasite vacuole. *Cell Microbiol* **22**, e13168 (2020).

878 39. R. F. Waller, M. B. Reed, A. F. Cowman, G. I. McFadden, Protein trafficking to the
879 plastid of Plasmodium falciparum is via the secretory pathway. *Embo Journal* **19**, 1794-
880 1802 (2000).

881 40. A. Adisa *et al.*, The Signal Sequence of Exported Protein-1 Directs the Green
882 Fluorescent Protein to the Parasitophorous Vacuole of Transfected Malaria Parasites.
883 *Journal of Biological Chemistry* **278**, 6532-6542 (2003).

884 41. S. M. Ganesan, A. Falla, S. J. Goldfless, A. S. Nasamu, J. C. Niles, Synthetic RNA-
885 protein modules integrated with native translation mechanisms to control gene
886 expression in malaria parasites. *Nat Commun* **7**, 10727 (2016).

887 42. K. Rajaram, H. B. Liu, S. T. Prigge, Redesigned TetR-Aptamer System To Control Gene
888 Expression in Plasmodium falciparum. *mSphere* **5** (2020).

889 43. S. H. Adjalley *et al.*, Quantitative assessment of Plasmodium falciparum sexual
890 development reveals potent transmission-blocking activity by methylene blue.
891 *Proceedings of the National Academy of Sciences* **108**, E1214-E1223 (2011).

892 44. A. P. AhYoung, A. Koehl, D. Cascio, P. F. Egea, Structural mapping of the ClpB
893 ATPases of Plasmodium falciparum: Targeting protein folding and secretion for
894 antimalarial drug design. *Protein Sci* **24**, 1508-1520 (2015).

895 45. M. El Bakkouri *et al.*, The Clp Chaperones and Proteases of the Human Malaria Parasite
896 Plasmodium falciparum. *Journal of Molecular Biology* **404**, 456-477 (2010).

897 46. E. Yeh, J. L. Derisi, Chemical Rescue of Malaria Parasites Lacking an Apicoplast
898 Defines Organelle Function in Blood-Stage Plasmodium falciparum. *PLoS Biology* **9**,
899 e1001138 (2011).

900 47. G. G. Van Dooren, V. Su, M. C. D'Ombrain, G. I. McFadden, Processing of an
901 Apicoplast Leader Sequence inPlasmodium falciparum and the Identification of a
902 Putative Leader Cleavage Enzyme. *Journal of Biological Chemistry* **277**, 23612-23619
903 (2002).

904 48. M. Zhang *et al.*, Uncovering the essential genes of the human malaria parasite
905 Plasmodium falciparum by saturation mutagenesis. *Science* **360** (2018).

906 49. E. Bushell *et al.*, Functional Profiling of a Plasmodium Genome Reveals an Abundance
907 of Essential Genes. *Cell* **170**, 260-272 e268 (2017).

908 50. M. E. Fichera, D. S. Roos, A plastid organelle as a drug target in apicomplexan
909 parasites. *Nature* **390**, 407-409 (1997).

910 51. E. L. Dahl, P. J. Rosenthal, Multiple antibiotics exert delayed effects against the
911 Plasmodium falciparum apicoplast. *Antimicrob Agents Chemother* **51**, 3485-3490 (2007).

912 52. N. I. Proellocks *et al.*, Characterisation of PfRON6, a Plasmodium falciparum rhoptry
913 neck protein with a novel cysteine-rich domain. *Int J Parasitol* **39**, 683-692 (2009).

914 53. S. A. Desai, D. J. Krogstad, E. W. McCleskey, A nutrient-permeable channel on the
915 intraerythrocytic malaria parasite. *Nature* **362**, 643-646 (1993).

916 54. S. A. Desai, R. L. Rosenberg, Pore size of the malaria parasite's nutrient channel.
917 *Proceedings of the National Academy of Sciences* **94**, 2045-2049 (1997).

918 55. M. Garten *et al.*, EXP2 is a nutrient-permeable channel in the vacuolar membrane of
919 Plasmodium and is essential for protein export via PTEX. *Nat Microbiol* **3**, 1090-1098
920 (2018).

921 56. D. A. Gold *et al.*, The Toxoplasma Dense Granule Proteins GRA17 and GRA23 Mediate
922 the Movement of Small Molecules between the Host and the Parasitophorous Vacuole.
923 *Cell Host Microbe* **17**, 642-652 (2015).

924 57. P. R. Sanders *et al.*, The N-terminus of EXP2 forms the membrane-associated pore of
925 the protein exporting translocon PTEX in Plasmodium falciparum. *The Journal of*
926 *Biochemistry* **165**, 239-248 (2019).

927 58. K. Hakamada, H. Watanabe, R. Kawano, K. Noguchi, M. Yohda, Expression and
928 characterization of the Plasmodium translocon of the exported proteins component
929 EXP2. *Biochemical and Biophysical Research Communications* **482**, 700-705 (2017).

930 59. M. D. Peraro, F. G. Van Der Goot, Pore-forming toxins: ancient, but never really out of
931 fashion. *Nature Reviews Microbiology* **14**, 77-92 (2016).

932 60. S. C. Charnaud, R. Kumarasingha, H. E. Bullen, B. S. Crabb, P. R. Gilson, Knockdown
933 of the translocon protein EXP2 in Plasmodium falciparum reduces growth and protein
934 export. *PLOS ONE* **13**, e0204785 (2018).

935 61. T. F. De Koning-Ward *et al.*, A newly discovered protein export machine in malaria
936 parasites. *Nature* **459**, 945-949 (2009).

937 62. J. M. Matz *et al.*, The Plasmodium berghei translocon of exported proteins reveals
938 spatiotemporal dynamics of tubular extensions. *Scientific Reports* **5**, 12532 (2015).

939 63. S. C. Charnaud *et al.*, Spatial organization of protein export in malaria parasite blood
940 stages. *Traffic* **19**, 605-623 (2018).

941 64. S. Nair *et al.*, Nutrient Limitation Magnifies Fitness Costs of Antimalarial Drug
942 Resistance Mutations. *Antimicrob Agents Chemother* **66**, e0152921 (2022).

943 65. A. Gupta *et al.*, Complex nutrient channel phenotypes despite Mendelian inheritance in a
944 Plasmodium falciparum genetic cross. *PLOS Pathogens* **16**, e1008363 (2020).

945 66. J. M. Matz *et al.*, In Vivo Function of PTEX88 in Malaria Parasite Sequestration and
946 Virulence. *Eukaryot Cell* **14**, 528-534 (2015).

947 67. S. A. Chisholm *et al.*, Contrasting Inducible Knockdown of the Auxiliary PTEX
948 Component PTEX88 in P. falciparum and P. berghei Unmasks a Role in Parasite
949 Virulence. *PLOS ONE* **11**, e0149296 (2016).

950 68. H. M. Kudyba, D. W. Cobb, J. Vega-Rodríguez, V. Muralidharan, Some conditions apply:
951 Systems for studying Plasmodium falciparum protein function. *PLOS Pathogens* **17**,
952 e1009442 (2021).

953 69. J. Birnbaum *et al.*, A genetic system to study Plasmodium falciparum protein function.
954 *Nature Methods* **14**, 450-456 (2017).

955 70. A. D. Roberts, S. C. Nair, A. J. Guerra, S. T. Prigge, Development of a conditional
956 localization approach to control apicoplast protein trafficking in malaria parasites. *Traffic*
957 **20**, 571-582 (2019).

958 71. A. Praznik *et al.*, Regulation of protein secretion through chemical regulation of
959 endoplasmic reticulum retention signal cleavage. *Nature Communications* **13** (2022).

960 72. A. Prasad, P. Mastud, S. Patankar, Dually localised proteins found in both the apicoplast
961 and mitochondrion utilize the Golgi-dependent pathway for apicoplast targeting in
962 Toxoplasma gondii. *Biology of the Cell* **113**, 58-78 (2021).

963 73. A. Florentin *et al.*, PfClpC Is an Essential Clp Chaperone Required for Plastid Integrity
964 and Clp Protease Stability in Plasmodium falciparum. *Cell Rep* **21**, 1746-1756 (2017).

965 74. A. Florentin, D. R. Stephens, C. F. Brooks, R. P. Baptista, V. Muralidharan, Plastid
966 biogenesis in malaria parasites requires the interactions and catalytic activity of the Clp
967 proteolytic system. *Proc Natl Acad Sci U S A* **117**, 13719-13729 (2020).

968 75. A. Mogk, B. Bukau, H. H. Kampinga, Cellular Handling of Protein Aggregates by
969 Disaggregation Machines. *Molecular Cell* **69**, 214-226 (2018).

970 76. I. Bouchnak, K. J. Van Wijk, Structure, function, and substrates of Clp AAA+ protease
971 systems in cyanobacteria, plastids, and apicoplasts: A comparative analysis. *Journal of*
972 *Biological Chemistry* **296**, 100338 (2021).

973 77. K. Pakos-Zebrucka *et al.*, The integrated stress response. *EMBO reports* **17**, 1374-1395
974 (2016).

975 78. M. Costa-Mattioli, P. Walter, The integrated stress response: From mechanism to
976 disease. *Science* **368** (2020).

977 79. M. B. Harbut *et al.*, Targeting the ERAD pathway via inhibition of signal peptide
978 peptidase for antiparasitic therapeutic design. *Proceedings of the National Academy of*
979 *Sciences* **109**, 21486-21491 (2012).

980 80. M. Zhang *et al.*, PK4, a eukaryotic initiation factor 2 (eIF2) kinase, is essential for the
981 development of the erythrocytic cycle of Plasmodium. *Proceedings of the National*
982 *Academy of Sciences* **109**, 3956-3961 (2012).

983 81. M. Zhang *et al.*, Inhibiting the Plasmodium eIF2α Kinase PK4 Prevents Artemisinin-
984 Induced Latency. *Cell Host & Microbe* **22**, 766-776.e764 (2017).

985 82. E. C. Gaynor, S. Te Heesen, T. R. Graham, M. Aebi, S. D. Emr, Signal-mediated
986 retrieval of a membrane protein from the Golgi to the ER in yeast. *Journal of Cell Biology*
987 **127**, 653-665 (1994).

988 83. M. Stornaiuolo *et al.*, KDEL and KKXX Retrieval Signals Appended to the Same
989 Reporter Protein Determine Different Trafficking between Endoplasmic Reticulum,
990 Intermediate Compartment, and Golgi Complex. *Molecular Biology of the Cell* **14**, 889-
991 902 (2003).

992 84. B. L. Tang, S. H. Wong, S. H. Low, W. Hong, Retention of a type II surface membrane
993 protein in the endoplasmic reticulum by the Lys-Asp-Glu-Leu sequence. *Journal of*
994 *Biological Chemistry* **267**, 7072-7076 (1992).

995 85. B. E. Sleebs *et al.*, Inhibition of Plasmepsin V Activity Demonstrates Its Essential Role in
996 Protein Export, PfEMP1 Display, and Survival of Malaria Parasites. *PLoS Biology* **12**,
997 e1001897 (2014).

998 86. S. H. Adjalley, M. C. S. Lee, D. A. Fidock, "A Method for Rapid Genetic Integration into
999 Plasmodium falciparum Utilizing Mycobacteriophage Bxb1 Integrase". (Humana Press,
1000 2010), 10.1007/978-1-60761-652-8_6, pp. 87-100.

1001 87. M. L. Jones *et al.*, A versatile strategy for rapid conditional genome engineering using
1002 loxP sites in a small synthetic intron in Plasmodium falciparum. **6**, 21800 (2016).

1003 88. S. Glushakova *et al.*, Exploitation of a newly-identified entry pathway into the malaria
1004 parasite-infected erythrocyte to inhibit parasite egress. *Scientific Reports* **7** (2017).

1005 89. A. I. Ahiya, S. Bhatnagar, J. M. Morrisey, J. R. Beck, A. B. Vaidya, Dramatic
1006 Consequences of Reducing Erythrocyte Membrane Cholesterol on Plasmodium
1007 falciparum. *Microbiol Spectr* **10**, e0015822 (2022).

1008 90. T. W. Kooij, M. M. Rauch, K. Matuschewski, Expansion of experimental genetics
1009 approaches for Plasmodium berghei with versatile transfection vectors. *Mol Biochem*
1010 *Parasitol* **185**, 19-26 (2012).

1011 91. C. J. Janse, J. Ramesar, A. P. Waters, High-efficiency transfection and drug selection of
1012 genetically transformed blood stages of the rodent malaria parasite Plasmodium berghei.
1013 *Nature Protocols* **1**, 346-356 (2006).

1014 92. R. S. Kent *et al.*, Inducible developmental reprogramming redefines commitment to
1015 sexual development in the malaria parasite Plasmodium berghei. *Nature Microbiology* **3**,
1016 1206-1213 (2018).

1017 93. M. A. Fierro *et al.*, An Endoplasmic Reticulum CREC Family Protein Regulates the
1018 Egress Proteolytic Cascade in Malaria Parasites. *mBio* **11** (2020).

1019 94. J. Schindelin *et al.*, Fiji: an open-source platform for biological-image analysis. *Nature*
1020 *Methods* **9**, 676-682 (2012).

1021 95. E. P. Rock *et al.*, Comparative analysis of the Plasmodium falciparum histidine-rich
1022 proteins HRP-I, HRP-II and HRP-III in malaria parasites of diverse origin. *Parasitology*
1023 **95**, 209-227 (1987).

1024 96. T. Blisnick *et al.*, Pfsbp1, a Maurer's cleft Plasmodium falciparum protein, is associated
1025 with the erythrocyte skeleton. *Mol Biochem Parasitol* **111**, 107-121 (2000).

1026 97. R. Hall *et al.*, Antigens of the erythrocytic stages of the human malaria parasite
1027 Plasmodium falciparum detected by monoclonal antibodies. *Molecular and Biochemical*
1028 *Parasitology* **7**, 247-265 (1983).

1029 98. M. Ponpuak *et al.*, A role for falcilysin in transit peptide degradation in thePlasmodium
1030 falciparumapicoplast. *Molecular Microbiology* **63**, 314-334 (2007).

1031 99. K. Matthews *et al.*, ThePlasmodiumtranslocon of exported proteins (PTEX)
1032 component thioredoxin-2 is important for maintaining normal blood-stage growth.
1033 *Molecular Microbiology* **89**, 1167-1186 (2013).

1034